

The nature of the plate interface and driving force of interseismic deformation in the New Zealand plate-boundary zone, revealed by the continuous GPS velocity field

Simon Lamb¹ and Euan Smith¹

Received 30 December 2012; revised 9 May 2013; accepted 14 May 2013; published 18 June 2013.

[1] New Zealand straddles the boundary between the Australian and Pacific plates. Cenozoic relative plate motion has resulted in a complex pattern of faulting and block rotation, with displacements on individual faults up to hundreds of kilometers. However, over periods of several years, GPS measurements show a remarkably smooth pattern of velocities. We show here using a new method of back slip analysis, that almost the entire plate-boundary continuous GPS velocity field can be predicted within measurement error from a simple model of elastic distortion due to deep slip on a *single* plate interface (megathrust in the Hikurangi and Putsegur subduction zones or fault through continental lithosphere beneath the Southern Alps) at the *relative plate motion rates*. This suggests that the main driving force of plate-boundary deformation is slip on the deeper moving part of the plate interface, *without* buried creep in localized shear zones beneath individual surface faults. The depth at which this deep slip terminates (locking point line) determines the width of deformation. Along the Hikurangi margin, there is also clockwise rotation of ~150 km long segment of the fore arc (Wairoa domain) at $4.5^\circ \pm 1$ Ma, relative to the Australian Plate, about a pole in western North Island; model residuals in the velocity field are mainly a result of incomplete averaging of the cycle of slow slip events on the plate interface, downdip of the locking point.

Citation: Lamb, S., and E. Smith (2013), The nature of the plate interface and driving force of interseismic deformation in the New Zealand plate-boundary zone, revealed by the continuous GPS velocity field, *J. Geophys. Res. Solid Earth*, 118, 3160–3189, doi:10.1002/jgrb.50221.

1. Introduction

[2] It has been long appreciated that where the boundary between two tectonic plates passes through continental lithosphere, deformation is distributed over a wide region up to several thousand kilometers wide [McKenzie and Jackson, 1983]. However, the dynamical controls on the pattern of deformation remain an important problem in geology. Thus, it is unclear whether deformation is driven mainly by some sort of underlying fluid-like flow in the lower crust or mantle [England and McKenzie, 1982; McKenzie and Jackson, 1983; England and Houseman, 1989; Lamb, 1994] or reflects the response of the brittle crust and mantle to forces along faults [Jackson, 2002; Lamb, 2002].

[3] Geodetic studies in many plate-boundary zones—for example, retriangulation and GPS measurements—show that at short time scales, much shorter than the seismic cycle and of the order of years to decades, the relative plate motion is accommodated by a smooth pattern of flow, whereas on longer time

scales, displacement is taken up by folding, faulting, and block rotation. In the last decade, continuous GPS networks have become sufficiently dense that it has been possible to resolve an intermediate behavior, where short-term flow is complicated by slip events over days or months (summarized in Wallace and Beavan [2010])—the so-called slow slip events (SSEs).

[4] One way of thinking about the different time scales of this deformation is in terms of the buildup of stress, and then failure of the lithosphere. In this view, the very short-term GPS pattern of flow directly reflects the stress loading of the elastic brittle part of the lithosphere, driven by motions at greater depth, which may be completely independent of the geometry of surface faults. Eventually, the brittle crust and/or mantle will reach failure, rupturing along the surface faults during earthquakes or SSEs. Thus, the slip on surface faults will be dictated by the requirement that the interseismic buildup of stress over several seismic cycles ultimately has to be relieved because the brittle part of the lithosphere has a finite strength, and this failure will occur wherever the brittle layer is closest to failure. In this case, GPS measurements potentially provide information about the nature of the driving forces of plate-boundary deformation. At deeper levels in the lithosphere, this strain may occur as distributed deformation.

¹Institute of Geophysics, Victoria University of Wellington, Wellington, New Zealand.

Corresponding author: S. Lamb, Institute of Geophysics, Victoria University of Wellington, PO Box 600, Wellington 6140, New Zealand.
(simon.lamb@vuw.ac.nz)

©2013. American Geophysical Union. All Rights Reserved.
2169-9313/13/10.1002/jgrb.50221

1.1. New Zealand Plate-Boundary Zone

[5] The New Zealand plate-boundary zone has a rich database of both campaign GPS and continuous GPS (Figure 1),

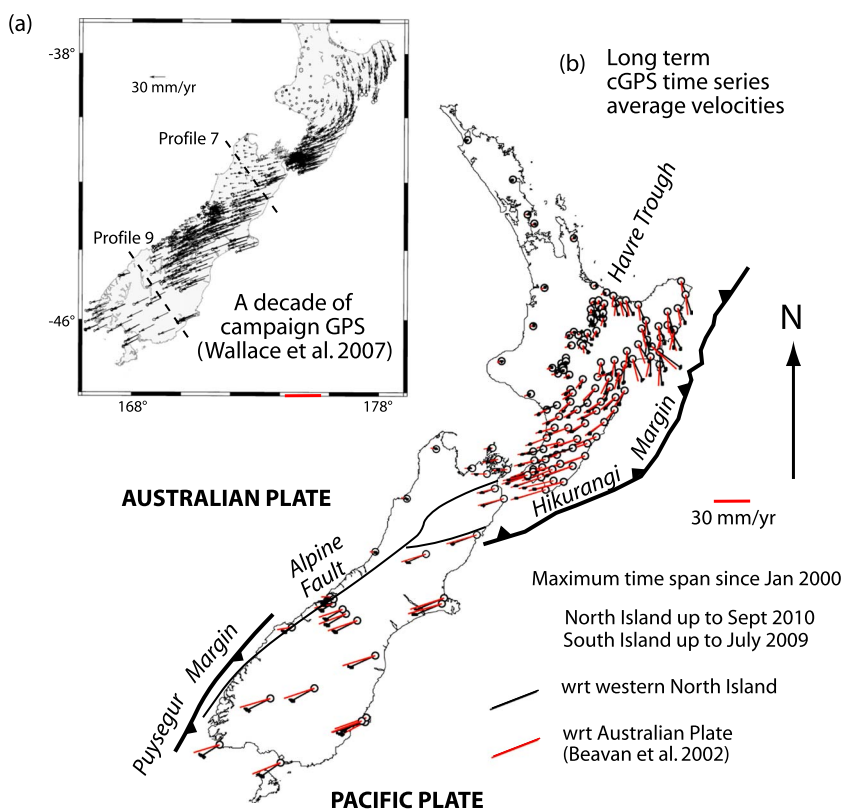


Figure 1. Map showing velocities, relative to Australian plate, derived from GPS, and the major tectonic features of the New Zealand plate-boundary zone. (a) Campaign GPS studies between 1992 and 2004 [Wallace et al., 2007] revealed a smooth pattern of flow accommodating the relative motion of the Pacific and Australian plates. Note the strong rotation of velocity vectors in North Island, which is a direct result of behind arc spreading in the north and compression farther south. Also shown are the locations of Profiles 7 and 9, modeled in this study using these data (see Figures 11b and 20a). (b) Long-term velocity solutions for continuous GPS (cGPS), relative to Australian plate (red) and western North Island (black). Circles are site locations. The cGPS sites are much sparser than those in campaign GPS studies (see Figure 1a), but they reveal essentially the same smooth pattern of flow accommodating the relative motion of the Pacific and Australian plates. Velocities are a best fit linear approximation to full available time series at any particular site. Small ellipses at the end of black vectors are 95% confidence errors reflecting the western North Island reference pole uncertainty.

as well as neotectonic studies of active fault movements (Figure 2). Here deformation in a broad zone of faulting and block rotation, up to 250 km wide, accommodates the obliquely convergent motion between the Australian and Pacific plates at ~40 mm/yr. There are three distinct tectonic settings, dominated by subduction of Pacific plate in the north (Hikurangi margin) and Australian plate in the south (Puysegur margin), with oblique continental collision on the Alpine Fault and in the Southern Alps between these two subduction zones. The subduction zones are well imaged by microseismicity, with tens of thousands of earthquakes $>M1.8$ in the last 20 years (www.geonet.org.nz). These show that the extent of the plate-boundary zone in the vertical dimension is similar to its horizontal scale, with Benioff zones extending to >600 km in the Hikurangi subduction zone and >200 km in the Puysegur subduction zone.

[6] In this paper, we show that almost the entire horizontal and vertical GPS velocity field in the New Zealand plate-boundary zone, averaged over 5–10 years, can be explained by deep slip on a single plate interface, which is either along a subduction zone or in continental lithosphere, and moving

at the relative plate motion. The key parameter that determines the width and pattern of deformation is the depth at which this deep slip terminates (the so-called locking point); at shallower levels, the relative plate motion is accommodated by elastic distortion in the brittle part of the lithosphere. Surface faults appear to play no role in this deformation, with no clearly resolvable evidence for marked velocity gradients across faults that might indicate localized buried creep in individual shear zones at depth. Thus, the number of parameters required to model most (90–95%) of the GPS velocity field in the plate-boundary is reduced to just those needed to define the locking point “line” along the plate interface.

[7] The Hikurangi margin is also affected by slow slip earthquakes (SSEs), lasting days to months with repeat times ranging from 1 to 6 years (see sections 5.2 and 6) [Wallace and Beavan, 2010]. We show that a simple model of incomplete averaging of the cycle of slow slip events (SSEs) on the subduction interface here, downdip of the locking point line, or where there are abrupt lateral transitions from locked to freely slipping, can account for any residuals in our model of the velocity field, particularly in the vertical motions.

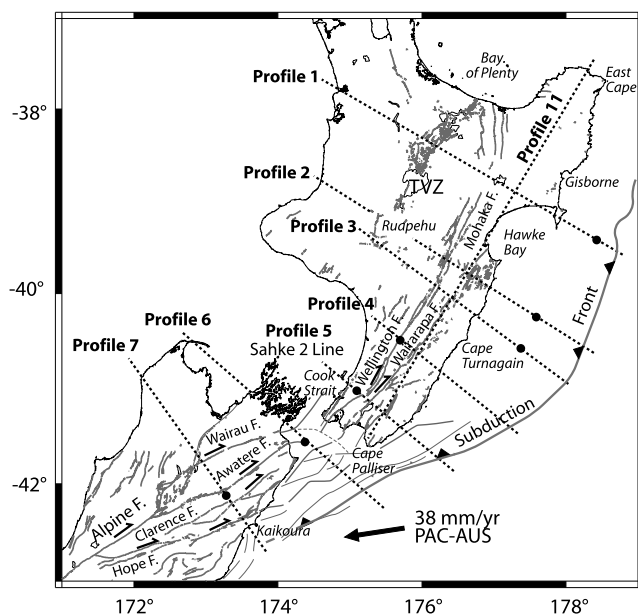


Figure 2. Detailed pattern of active faulting (Holocene and recent) in the central and northern part of the New Zealand plate-boundary zone (see Figure 6 for location). Most faults are reverse (except in the northern part of North Island) and have a dextral component of strike-slip motion, with slip rates in the range 3–30 mm/yr. Also shown are the locations of Profiles 1–7 and 11, analyzed in this study, spanning the zone of complex and rapid long-term faulting. However, the interseismic velocity field from cGPS time series is modeled in this study by a single locking point (black dots show horizontal projection of the locking point) on the underlying subduction megathrust (see text). In other words, surface faults appear not to exist during the interseismic period, and hence play no role in the interseismic velocity field. The latter is determined by deep slip on the plate interface.

2. GPS Data

2.1. Campaign Data

[8] There have been numerous regional GPS surveys in the New Zealand plate-boundary zone since 1991 (Figure 1a), conducted by GNS Science. These surveys were specifically designed to constrain crustal deformation on a length scale of tens of kilometers, involving several hundred stations with multiple sessions of occupation generally for 18–24 h; full details of the methodology are given in published analyses of the results [Beavan *et al.*, 1999; Darby and Beavan, 2001; Wallace *et al.*, 2004, 2007].

[9] Unfortunately, velocity solutions for individual stations are usually not published (except for the Wellington region in Darby and Beavan [2001]), and so any further analysis of these campaign GPS surveys is restricted to where the data have been projected on to selected published profiles. A further difficulty exists, because it is sometimes unclear about the details of the frame of reference for the published profile velocities. For these reasons, we only use the campaign data for illustrative purposes, to show its general consistency with more recent continuous GPS measurements.

2.2. Geonet Continuous GPS Data

[10] Over the last decade, a network of continuous GPS stations (referred to as cGPS) has been installed in both North and South Islands, spanning the plate-boundary zone (Figure 1b), and the data are available on a daily basis online (<http://www.geonet.org.nz/resources/gps/>). These data have been processed using standard methods, making atmospheric and network

wide corrections, and are reported in the International Terrestrial Reference Frame (ITRF) 2000. There has been a program of densifying the network along the eastern side and in central North Island, with ~20 km spacing, specifically designed to monitor crustal motions associated with volcanic processes and slow slip earthquakes on the subduction megathrust [Wallace and Beavan, 2010]. Elsewhere in North Island, and for most of South Island, the network is much sparser with ~100 km spacing, except for a detailed transect across the central part of the Southern Alps.

[11] We have determined velocity solutions (Table 1 and Figure 1b) for both the horizontal and vertical components of station motion, by fitting long-term linear trends to the daily solutions, over the maximum time span available (2–10 years), making allowance for any original network-wide inconsistencies in the data. Formal errors for the velocities are not easily determined because individual daily positions are correlated. Nonetheless, the velocity error will be small compared to the other uncertainties arising when used for modeling [see Beavan *et al.*, 2002]. An alternative measure of the quality of the fits is given by the root mean square (rms) misfit, generally <1 mm/yr for components of velocities averaged over periods >5 years.

[12] We caution that the real measure of accuracy of the GPS velocity field, as a representation of horizontal crustal motion relative to some external reference frame (see section 2.3) will be much higher than this, and most likely of the order of 1–2 mm/yr, reflecting uncertainties in the choice of reference frames. Uncertainties in the vertical velocity are up to an order of magnitude higher than this, especially for

Table 1. Full Time Series cGPS Velocities in This Study With Respect to the Australian Plate Reference Frame [Defined by Beavan et al., 2002]

Site Name ^a	Longitude (°E)	Latitude (°N)	V _e ^b mm/yr	V _n ^b mm/yr	V _z ^b mm/yr	rmsE ^c mm/yr	rmsN ^c mm/yr	rmsZ ^c mm/yr	Start day ^d	End day ^e
AHTI	178.0460	-38.4114	8.9	-26.9	0.4	1.2	0.6	9.8	3449	3935
AKTO	176.4612	-40.5398	-28.7	-11.3	-3.3	0.8	0.2	3.1	2308	3935
ARTA	176.1364	-38.6176	0.8	-8.1	-3.8	0.7	0.5	6.2	3232	3935
AUCK	174.8344	-36.6028	-2.3	-1.8	1.1	0.1	0.0	0.6	1	3935
AVLN	174.9329	-41.1964	-23.7	-7.8	-0.4	0.6	0.8	3.8	2246	3935
BHST	176.0632	-39.4892	-7.1	-9.1	0.5	0.6	0.4	5.9	3093	3935
BIRF	176.2461	-40.6798	-30.0	-8.9	-4.1	0.4	0.4	2.8	1853	3935
BLUF	168.2921	-46.5851	-28.8	-10.6	0.5	0.2	0.2	2.9	1531	3482
BNET	170.1901	-43.8625	-27.4	-9.9	3.2	1.0	0.6	9.2	1872	3482
BTHL	175.1365	-41.3405	-32.1	-9.6	-2.0	5.9	2.6	24.5	3301	3935
CAST	176.2016	-40.9098	-30.8	-10.4	-3.0	0.6	0.3	5.9	2232	3935
CKID	177.0764	-39.6579	-10.1	-16.5	3.2	0.3	0.2	2.3	2335	3935
CLIM	175.1455	-41.1447	-26.3	-9.0	-1.8	0.9	0.6	4.5	2118	3935
CMBL	174.2138	-41.7490	-27.2	-7.2	0.5	0.3	0.2	2.2	1488	3482
CNCL	169.8559	-43.6662	-18.5	-4.8	4.7	0.1	0.1	2.0	35	3482
CNST	178.2111	-38.4880	-4.8	-20.2	-1.1	0.4	0.3	4.2	2844	3935
CORM	175.7496	-36.8654	-2.2	-0.6	0.3	0.3	0.1	2.1	1225	3935
DNVK	176.1667	-40.2989	-18.7	-10.5	-2.2	0.3	0.2	2.4	1013	3935
DUND	170.5972	-45.8837	-33.0	-11.3	-0.9	0.3	0.4	4.0	2062	3482
DUNT	170.6294	-45.8143	-31.8	-11.5	0.8	0.3	0.3	2.4	1	3100
DURV	173.9216	-40.8018	-9.3	-1.1	-1.7	0.5	0.2	2.5	1895	3935
GISB	177.8860	-38.6353	-4.7	-17.8	-1.4	0.1	0.1	1.7	909	3935
GLDB	172.5296	-40.8266	-5.8	1.2	-1.2	0.3	0.3	2.6	1493	3935
GNBK	175.2381	-40.0803	-13.6	-5.1	0.1	0.4	0.3	4.1	3008	3935
GRAC	174.9170	-41.2351	-26.7	-7.6	-0.9	0.4	0.4	2.7	25	2430
GRNG	175.4593	-39.9763	-13.7	-4.7	0.1	0.3	0.2	3.2	2729	3935
HAAS	168.7856	-44.0732	-15.4	-2.1	1.1	0.3	0.3	4.7	1635	3482
HAMT	175.1092	-37.8068	-3.8	-0.5	0.5	0.2	0.1	2.1	1229	3935
HANA	177.5694	-38.6868	-2.0	-17.7	1.6	0.3	0.3	4.9	2776	3935
HAST	176.7266	-39.6170	-8.8	-13.9	-3.6	0.2	0.1	1.7	992	3935
HIKB	178.3034	-37.5610	1.8	-17.5	0.3	0.2	0.2	2.4	1232	3935
HOKI	170.9843	-42.7129	-6.2	-0.1	3.7	0.1	0.1	1.5	1	3482
HOLD	175.5152	-40.8972	-25.4	-8.8	-1.2	1.9	0.6	10.8	2631	3935
HORN	170.1055	-43.7773	-24.9	-8.3	4.3	2.0	0.8	20.4	1054	2700
KAHU	176.8763	-39.7938	-15.0	-13.2	-1.5	0.3	0.2	2.2	2301	3935
KAIK	173.5337	-42.4255	-31.4	-9.4	-0.8	0.3	0.3	3.0	1492	3482
KAPT	174.9098	-40.8609	-16.3	-3.1	0.9	0.4	0.3	1.9	1622	3935
KARA	169.7752	-43.6084	-13.5	-2.0	2.9	0.2	0.1	1.5	35	3100
KAWK	176.4228	-39.4240	9.8	2.4	-6.5	3.9	3.6	38.5	3805	3935
KERE	176.3701	-39.6432	-12.2	-13.4	-5.3	1.8	0.6	7.1	2329	3935
KOKO	177.6678	-39.0161	-4.5	-20.4	-0.3	0.2	0.1	2.0	1769	3935
KORO	175.4241	-40.4093	-19.8	-5.2	-3.4	0.2	0.2	3.4	2727	3935
KTIA	173.2731	-35.0689	-3.5	-0.1	0.4	0.3	0.3	4.4	2853	3935
KUTA	177.0698	-39.1723	-6.1	-20.9	-4.2	2.7	2.1	22.4	3749	3935
LEVN	175.2406	-40.5888	-22.5	-8.1	-3.4	0.5	0.3	6.7	3132	3935
LEXA	169.3083	-45.2310	-31.8	-10.3	0.3	0.8	0.4	5.5	1538	3482
LEYL	176.9367	-39.3323	-5.2	-17.3	-2.1	0.3	0.3	3.8	2716	3935
LKTA	172.2663	-42.7834	-25.4	-7.9	2.3	0.3	0.7	3.8	1495	3482
LYTT	172.7222	-43.6058	-35.0	-11.2	1.0	0.2	0.3	2.3	78	3200
MAHA	173.7938	-41.2914	-17.0	-0.2	1.3	2.5	1.8	23.0	3607	3935
MAHI	177.9070	-39.1526	-2.2	-21.8	-0.7	0.6	0.3	4.5	2773	3935
MAHO	174.8541	-38.5130	-3.8	-0.3	-1.6	0.3	0.1	2.5	1494	3935
MANG	175.5749	-40.6687	-24.4	-6.0	-0.9	3.3	1.1	9.1	1869	3935
MAST	175.5846	-41.0620	-29.9	-10.3	-3.0	0.2	0.1	2.4	1099	3935
MATW	177.5262	-38.3338	-1.8	-15.7	2.7	0.3	0.1	2.1	1560	3935
MAVL	168.1182	-45.3665	-31.7	-9.4	-4.7	1.5	1.3	20.8	2900	3482
MCNL	176.6965	-39.4442	-8.0	-16.9	-5.3	0.5	0.3	5.7	3069	3935
MQZG	172.6547	-43.7027	-35.1	-11.0	2.6	0.1	0.2	1.5	6	3482
MTBL	175.5362	-40.1814	-17.2	-8.7	-2.9	0.3	0.2	4.0	3011	3935
MTJO	170.4649	-43.9857	-29.8	-10.5	1.2	0.2	0.1	2.0	227	3482
MTQN	175.2414	-41.0016	-29.9	-5.8	-4.4	4.1	3.5	34.9	3692	3935
NLSN	173.4337	-41.1835	-9.0	0.1	-1.7	0.2	0.2	2.3	1500	3935
NMAI	176.8066	-39.0970	-2.6	-17.0	0.1	1.4	1.2	5.4	3019	3935
NPLY	174.1182	-39.1826	-4.8	-0.6	-0.2	0.3	0.2	3.1	1175	3935
NRRD	175.7613	-40.3854	-24.0	-8.2	-6.4	1.8	0.7	7.6	3008	3935
OHIN	175.7907	-39.9183	-12.0	-10.5	4.0	0.5	0.3	5.4	3168	3935
OKOH	174.0603	-41.0193	-16.1	-3.2	2.4	2.5	2.0	18.9	3607	3935
OPTK	177.3076	-38.0465	2.1	-17.0	2.6	1.1	0.7	11.5	3519	3935

LAMB AND SMITH: MODELING GPS VELOCITIES IN NEW ZEALAND

Table 1. (continued)

Site Name ^a	Longitude (°E)	Latitude (°N)	Ve ^b mm/yr	Vn ^b mm/yr	Vz ^b mm/yr	rmsE ^c mm/yr	rmsN ^c mm/yr	rmsZ ^c mm/yr	Start day ^d	End day ^e
OTAK	175.1704	-40.8165	-21.0	-5.0	-1.4	0.5	0.4	6.0	2837	3935
OUSD	170.5109	-45.8695	-31.2	-11.4	1.3	0.2	0.2	2.0	1	2900
PAEK	174.9521	-41.0218	-20.5	-5.7	2.8	0.2	0.2	2.1	101	3935
PALI	175.2548	-41.5692	-36.5	-9.6	-3.6	0.4	0.4	4.1	2637	3935
PARI	177.8833	-38.9226	1.5	-20.0	-3.9	0.5	0.3	4.3	2770	3935
PARW	175.4269	-41.3815	-35.5	-9.1	-4.0	0.3	0.2	2.6	1657	3935
PAWA	176.8639	-40.0331	-13.5	-16.6	-1.1	0.2	0.1	2.3	1909	3935
PNUI	176.2005	-39.9168	-17.6	-10.0	-7.7	2.2	0.4	9.5	2372	3935
PORA	176.6352	-40.2664	-20.4	-13.7	-3.6	0.6	0.2	2.8	2275	3935
PRTU	177.6979	-38.8142	25.1	-24.0	0.8	1.6	0.8	12.0	3517	3935
PTOI	175.9993	-40.6011	-28.4	-9.2	-4.0	0.9	0.4	5.9	2272	3935
PUKE	178.2574	-38.0714	3.5	-17.9	1.6	0.2	0.1	2.1	1508	3935
PYGR	166.6807	-46.1662	-26.4	-7.9	0.3	0.7	1.1	8.3	2677	3482
QUAR	169.8158	-43.5317	-10.1	-0.8	-0.4	0.1	0.2	3.5	35	3482
RAHI	177.0861	-38.9162	-1.0	-17.9	0.7	0.6	0.7	6.8	3061	3935
RAWI	177.4154	-38.4956	4.8	-19.7	3.4	1.5	1.7	10.3	3448	3935
RDLV	175.4043	-41.1869	-31.2	-10.9	-2.9	2.0	1.0	11.4	3301	3935
RGAR	176.3430	-38.5620	-2.9	-7.6	-1.5	0.3	0.2	4.3	2867	3935
RGAW	176.8962	-38.0032	3.3	-15.6	2.7	0.9	0.6	6.6	3370	3935
RGCR	176.3780	-38.1047	-1.7	-5.4	-2.8	0.5	0.2	3.8	2600	3935
RGHL	176.3523	-38.2519	-4.8	-7.6	-18.3	3.3	1.1	7.0	3260	3933
RGHR	176.2880	-38.3858	-5.1	-6.0	-7.3	0.6	0.3	4.3	2602	3935
RGKA	176.2441	-38.0201	-1.9	-2.9	1.1	0.3	0.2	2.9	2320	3935
RGKW	176.7728	-38.0525	-0.8	-12.9	-0.1	0.7	0.4	6.1	3254	3935
RGLI	176.3857	-38.0033	-1.5	-5.0	-1.2	0.2	0.2	2.6	2146	3935
RGMK	176.4671	-38.1383	-1.3	-9.3	-15.7	0.4	0.2	3.1	1740	3935
RGMT	176.7247	-37.9155	-0.9	-11.0	11.7	0.5	0.3	4.0	2859	3935
RGON	176.2323	-38.2566	7.8	-7.6	-16.2	1.4	0.6	8.2	3524	3935
RGOP	176.5561	-37.8459	-5.6	-3.0	5.2	0.3	0.2	3.2	2609	3935
RGRE	176.5212	-38.0573	-3.3	-6.9	-2.1	0.4	0.3	4.5	2595	3935
RGR	176.5146	-38.3389	-2.7	-8.4	-0.3	0.4	0.3	4.0	2904	3935
RGTA	176.5061	-38.2338	-4.3	-5.7	-10.1	0.9	0.6	4.7	2882	3935
RGUT	176.1942	-38.1766	0.7	-4.8	-2.7	0.3	0.1	3.0	2176	3935
RGWV	176.2109	-38.3526	-0.6	-8.4	-14.6	1.2	1.0	10.7	3535	3935
RIPA	176.4925	-39.1655	-2.4	-11.8	1.2	0.2	0.2	2.8	1512	3935
SNST	177.3475	-38.7796	7.8	-20.2	3.0	1.7	1.4	14.4	3446	3935
TAKP	175.9629	-40.0616	-13.8	-8.1	-2.3	0.3	0.2	3.3	1491	3935
TAUP	176.0810	-38.7427	2.3	-6.7	4.7	0.1	0.1	1.5	811	3935
TAUW	178.0059	-38.1624	1.8	-22.0	3.8	1.9	1.3	14.0	3518	3933
TEMA	175.8905	-41.1066	-31.6	-11.0	-3.5	0.4	0.2	3.2	2633	3935
TGHO	175.9963	-38.8129	-2.0	-5.9	-1.4	1.2	0.7	10.5	3278	3935
TGHR	175.7119	-38.6781	-4.8	-1.5	1.8	0.3	0.2	3.1	2320	3935
TGOH	176.0475	-38.8458	1.4	-8.9	4.7	0.3	0.2	3.3	2334	3935
TGRA	175.7701	-38.8634	-7.2	-2.0	3.5	0.4	0.2	3.2	2293	3935
TGTK	175.8108	-38.6110	-3.6	-1.4	0.8	0.3	0.2	2.6	2328	3935
TGWH	175.9390	-38.6734	-1.2	2.3	-0.7	0.4	0.3	3.9	2594	3935
THAP	175.7856	-39.6825	-9.5	-5.9	3.5	0.5	0.4	7.0	3093	3935
TINT	175.8857	-40.7760	-28.9	-9.0	-5.4	0.4	0.3	2.8	2287	3935
TKAR	177.8114	-38.4375	2.9	-19.7	13.3	5.0	2.5	46.4	3806	3935
TORY	174.2801	-41.1916	-14.7	-1.6	0.7	0.5	0.4	2.8	1937	3935
TRAV	175.6879	-41.3980	-36.1	-9.4	-4.2	0.2	0.2	2.2	2000	3935
TRNG	176.2609	-37.7288	-1.1	-1.8	1.5	0.2	0.1	1.7	1144	3935
UTKU	175.8314	-39.7454	-9.9	-7.1	5.2	0.7	0.4	6.3	3240	3935
VGFW	175.5525	-39.2550	-4.3	-1.7	0.1	0.4	0.3	4.2	1540	3935
VGKR	175.6413	-39.0944	-4.7	-3.1	-0.3	0.6	0.4	4.4	1887	3935
VGMO	175.7543	-39.4074	-6.5	-4.0	2.6	0.3	0.3	4.2	1916	3935
VGMT	175.4705	-39.3846	-6.4	-1.1	1.7	0.2	0.2	2.1	1858	3935
VGOB	175.5422	-39.1998	-3.8	-1.9	0.0	0.3	0.2	4.4	1502	3935
VGOT	175.6651	-39.1631	-5.1	-2.7	-0.9	1.2	0.6	6.6	2351	3935
VGPK	175.3464	-39.2893	-5.8	-0.8	1.5	0.2	0.1	2.9	1847	3935
VGTR	175.5483	-39.2984	-5.4	-1.3	1.1	0.6	0.6	6.5	1868	3935
VGTS	175.6089	-39.2773	-5.6	-1.7	1.1	1.4	0.8	7.1	1902	3935
VGWH	175.5890	-39.2824	-5.2	-1.7	1.4	1.4	0.7	7.0	1882	3935
VGWN	175.5979	-39.3269	-5.0	-2.0	1.8	0.5	0.6	4.9	1599	3935
WAHU	177.2344	-39.0772	6.2	-23.1	0.6	0.9	0.6	8.9	3446	3935
WAIM	170.9203	-44.6557	-33.4	-10.6	-0.3	0.4	0.2	3.0	1812	3482
WAKA	169.8853	-43.5840	-16.0	-1.6	2.7	0.1	0.2	2.1	306	3482
WANG	174.8214	-39.7869	-6.6	-1.6	0.2	0.1	0.1	1.4	1203	3935
WARK	174.6628	-36.4344	-1.7	-0.9	1.2	0.6	0.6	8.7	3326	3935
WEST	171.8062	-41.7447	-6.3	0.6	-0.6	0.3	0.2	2.3	1727	3935

Table 1. (continued)

Site Name ^a	Longitude (°E)	Latitude (°N)	V_e^b mm/yr	V_n^b mm/yr	V_z^b mm/yr	rmsE ^c mm/yr	rmsN ^c mm/yr	rmsZ ^c mm/yr	Start day ^d	End day ^e
WGTN	174.8059	-41.3235	-26.9	-7.8	0.7	0.1	0.0	0.6	1	3935
WGTT	174.7816	-41.2904	-25.1	-6.7	-1.4	0.2	0.2	1.5	5	3935
WHKT	177.0139	-37.9817	3.9	-15.8	1.6	0.9	0.5	6.6	3369	3935
WHNG	174.3146	-35.8038	-2.8	-0.3	1.1	0.1	0.1	1.6	1195	3935
WITH	173.9843	-41.5606	-18.9	-4.8	4.6	2.2	1.4	15.1	3601	3935
WMAT	178.4087	-37.8250	2.9	-21.1	0.0	2.6	2.6	23.1	3726	3935
WPAW	176.5430	-39.8959	-18.4	-11.4	-6.2	0.3	0.2	3.4	2302	3935
WPUK	176.4406	-40.0642	-20.2	-9.2	-5.1	0.4	0.2	3.2	2301	3935

^aSite name is that used for Geonet cGPS network (www.geonet.org.nz).

^b V_e is toward East, V_n is toward North, V_z is upward.

^cRoot mean square residual to linear fit for full time series used.

^dStart day is 3 January 2000.

^eEnd day is in July 2009 for South Island and September 2010 for North Island.

cGPS time series less than about 5 years. In our analysis, because we do not attempt to formally model the data in a least squares sense, but rather search for solutions which are a representation of the data at some chosen misfit level (say <2 mm/yr), we only use the rms fit as a guide to the accuracy of the station horizontal velocity.

[13] For the oldest sites, we start our cGPS time series on 3 January 2000—since then, there has been a steady program of expanding the cGPS network. In July 2009, an ~120 km long segment of the megathrust in the Puysegur subduction zone, offshore southwestern South Island, ruptured in a M_w 7.8 earthquake, with a main shock hypocenter at a depth of about 30 km. Elastic rebound ranging from a few millimeters to over 3 m was observed at cGPS stations in South Island, up to 300 km away from the epicenter, with subsequent and ongoing displacement of several millimeters per year [Beavan *et al.*, 2010b], which has progressively decayed with time. For this reason, we only use cGPS data prior to July 2009 for South Island stations. For North Island, we only use cGPS time series prior to the $M7$ Darfield earthquake in September 2010.

2.3. Plate Reference Frame

[14] Beavan *et al.* [2002] used GPS sites in the interiors of the Australian and Pacific plates to determine the Euler poles for instantaneous Pacific and Australian plates relative to ITRF 2000, on a time scale of a decade. This directly gives the instantaneous Euler pole for the relative motion of the Pacific/Australian plates.

[15] Reference frames play a role in our analysis of the GPS data in two ways. First, they are used to calculate the horizontal velocities in a plate reference. Second, they are used to calculate the total motion across the plate-boundary zone required by plate tectonics. For this reason, the uncertainties in the reference frames tend to cancel each other out, when modeling the horizontal velocities, because they affect both these parts of the calculation in a similar way. However, these uncertainties play a role in model predictions of the vertical velocities, which do not require a horizontal plate reference frame. Thus, the vertical velocities can be used to test the accuracy of the horizontal reference frame.

[16] In this study, all horizontal velocities are given in the Australian plate reference frame (Table 1 and Figure 2), using the relevant Euler poles and Pacific/Australian plate motion from Beavan *et al.* [2002]. Sites along the east coast

of South Island have velocities within ~2 mm/yr of Pacific Plate. Sites in western North Island and along the west coast of South Island are close to stable Australian plate, with velocities ≤ 5 mm/yr. In fact, they define a remarkably good reference frame themselves, which requires ~75% lower velocity across the plate-boundary (Figure 2).

3. Back-Slip Models of Elastic Strain Accumulation in the New Zealand Plate-Boundary Zone

3.1. Faults and Earthquakes

[17] There is no evidence for surface creeping motion on any of the major faults in the New Zealand plate-boundary zone, but rather a historical record of earthquake rupture, recorded in incremental offsets of geomorphic features, detailed stratigraphy in fault trenching data, and uplift of marine and fluvial terraces [Beanland *et al.*, 1992; Berryman *et al.*, 2011; Cowan, 1990; Little *et al.*, 1998, 2009], with repeat times of the order of hundreds to thousands of years. This is strong evidence that the short-term deformation in the New Zealand plate-boundary zone on the time scale of years to decades can be thought of as interseismic deformation and largely represents elastic strain that will be redistributed during future fault rupture in earthquakes.

3.2. Back Slip Model for Interseismic Deformation

[18] Savage [1983] suggested that interseismic strain can be modeled in terms of a characteristic earthquake cycle on the plate interface, where the coseismic deformation (together with postseismic relaxation) along the entire plate interface relieves all the strain that has accumulated in the previous interseismic period (Figure 3). The basic assumption here is that (1) postseismic relaxation occurs over a short time compared to the length of the interseismic cycle and (2) the long-term deformation in the bounding plates is small. Thus, the steady state motion is free slip along the entire plate interface, and the interseismic strain is merely this steady state motion minus the coseismic deformation, together with postseismic relaxation, referred to as “back slip” on a virtual fault. The results for a general slip vector, and their sensitivity to fault geometry, have been thoroughly explored [Bevis and Martel, 2001; Kanda and Simons, 2012].

[19] Savage [1983] only considered a planar fault for his back slip calculations (Figure 3), but his method has subsequently been generalized to curved faults, subdivided into

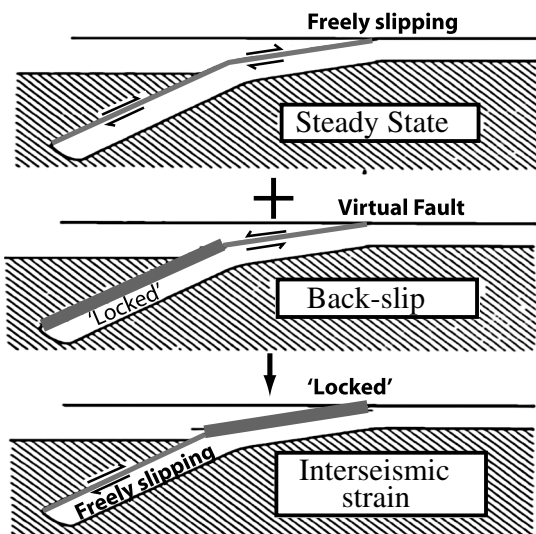


Figure 3. The principles of the “back slip method” after Savage [1983] for a subduction zone. This assumes a characteristic seismic cycle for the subduction zone, with a long-term steady state solution. The part of the fault that is not moving during the interseismic period is referred to as the “virtual fault.” During earthquakes, the virtual fault ruptures. The back slip is defined as the elastic rebound associated with the coseismic slip and postseismic relaxation that would occur on the virtual fault if displacement has the opposite sense to the actual coseismic and postseismic relaxation slip. In this case, the interseismic elastic deformation is the steady state solution plus the back slip.

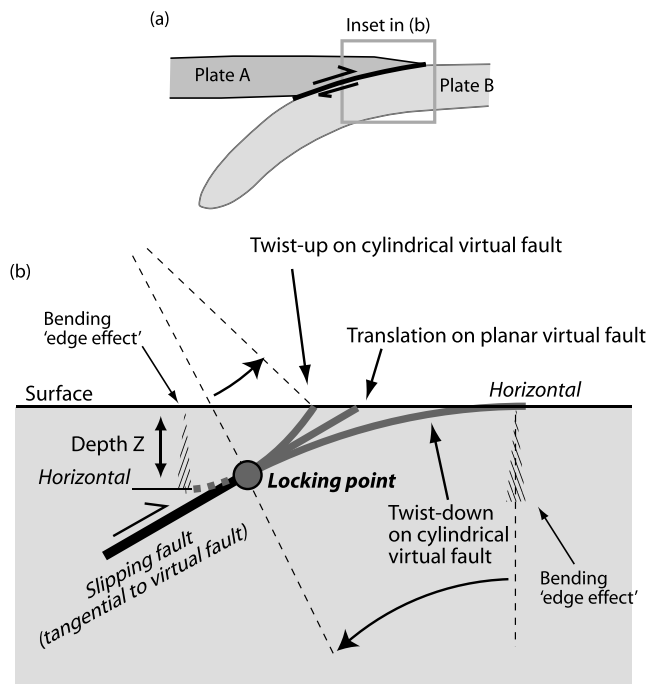
numerous planar patches [Beavan *et al.*, 1999; Darby and Beavan, 2001; McCaffrey *et al.*, 2000; McCaffrey, 2002; McCaffrey *et al.*, 2007; Wallace *et al.*, 2004, 2007, 2012a]. In this case, there is no obvious steady state solution, because blocks separated by a general nonplanar fault cannot slide past each other without internal deformation (Bevis [1986], and see further on). The problem is further increased in plate-boundary zones, such as New Zealand (Figures 1 and 2), where there is a wide zone of active surface deformation, and so coseismic deformation on any particular surface fault cannot be simply thought of as relieving all the interseismic plate-boundary stress/strain accumulation. In all these cases, there is no clear physical basis for the back slip model, and it remains somewhat paradoxical, because calculating the back slip requires a detailed knowledge of the geometry of the part of the plate interface that is not slipping during the interseismic period, and which, by definition, should not determine the interseismic velocity field [Vergne *et al.*, 2001].

[20] Despite all these problems, the back slip approach is often able to fit within error of the horizontal velocities [McCaffrey *et al.*, 2000; McCaffrey, 2005; McCaffrey *et al.*, 2007]. Darby and Beavan [2001] used a simple 2-D back slip model to analyze the available campaign GPS data in a profile across the onshore part of Hikurangi margin near Wellington. They could fit the horizontal velocities within their uncertainties (1–2 mm/yr) with a subduction megathrust that is freely slipping below a depth of ~29 km and locked at shallower depths, so that the locking point lies beneath the west coast near Wellington.

3.3. Variable Fault Coupling

[21] Darby and Beavan [2001] introduced extra degrees of freedom into their back slip modeling by considering the possibility that the plate interface slips at some fraction of the relative plate motion, referred to as partial slip. This is described by a “coupling factor,” where the coupling factor is 1—partial slip. Thus, the coupling factor is 0 if the fault slips at the relative plate motion (i.e., freely slipping), but it is 1 if the fault is locked. In fact, Darby and Beavan [2001] found that introducing a variable coupling factor did not significantly improve the fit to the horizontal velocities in their models.

[22] The physical basis of a variable coupling factor is unclear. It is sometimes assumed [Darby and Beavan, 2001; Wallace *et al.*, 2004, 2007] that a variable coupling factor must



Three possible geometries for steady state fault slip

Figure 4. (a) Schematic cross section of the plate interface at a subducting plate margin. Between big earthquakes, the shallow parts of the plate interface are locked, and here elastic strain/stress accumulates in the interseismic period. Key to the back slip model (see Figure 3) [Savage, 1983] for interseismic deformation is the existence of a long-term steady state slip on the plate interface to which the elastic velocity field associated with back slip on a virtual fault is added. (b) It is not generally recognized that steady state slip on a fault can only occur for a limited range of fault geometries. Thus, (thick grey lines) the virtual fault must be one of three geometries: (1) planar, or (2) concave cylindrical, resulting in a “twist-up,” or (3) convex cylindrical, resulting in a “twist-down.” The maximum depth of the virtual fault is called the locking point. In all cases, the virtual fault at the locking point is tangential to the part of the fault (thick black line) that is slipping during the interseismic deformation. Potential “edge effects,” at the ends of the model, where a twist becomes a translation, are shown by obliquely ruled triangular regions—these are likely to have a negligible effect on the surface velocity field, given the very low curvatures involved (see text).

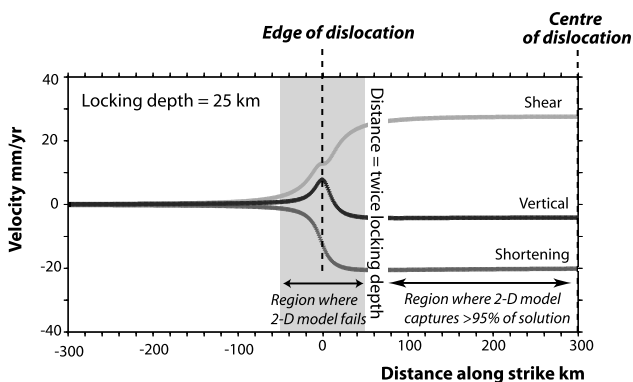


Figure 5. Diagram showing a surface velocity profile running along the strike of a dipping buried fault with finite lateral extent, modeled as a “twist-down” with a locking point depth of 25 km, typical of the southern part of the Hikurangi margin determined in this study. The profile lies above the “locked” part of the fault, 50 km horizontally (and updip) from the surface projection of the locking point. This shows that velocities at lateral distances more than about twice the locking depth are unaffected by the presence of the “edge” or end of the dislocation. This shows that assuming the buried fault is of infinite extent along strike (i.e., 2-D approximation), is a very good description, capturing >95% of the actual velocity field.

occur at the transition between locked and freely slipping, representing some sort of edge effect. However, finite element models of elastic deformation associated with buried slip show only a barely resolvable transition zone from fully locked to freely slipping at the full rate [Ader *et al.*, 2012], so that ignoring it is a good approximation to the actual elastic behavior.

[23] Partial coupling might also reflect much smaller scale patches of both freely slipping and locked portions of the fault, resulting in a lower average slip on the scale of the modeling [Wallace *et al.*, 2004]. However, the discovery in the last ~10 years, with cGPS, of slow slip events (SSEs) over periods of days to months, with a return time of a few years [e.g., Schwartz and Rokosky, 2007; Wallace and Beavan, 2010; Wallace *et al.*, 2012b], indicates an important process that can be accounted for in terms of a variable coupling factor. This is because the cGPS sites have been running for relative short periods, and so a coupling factor less than 1 is a way of taking this into account by quantifying incomplete averaging of the SSE cycle between the start and end times of individual cGPS time series (see section 5.2). The longer time periods of repeated GPS campaigns, up to nearly 15 years, seem to have effectively averaged out SSEs [Wallace and Beavan, 2010].

3.4. Multi-Block Models of Deformation With Partial Coupling

[24] Despite the success of Darby and Beavan’s [2001] back slip model, its main justification remains unclear because of the abundant evidence for significant long-term internal deformation in the overlying Australian plate (Figure 2 and see previous discussion). For example, the biggest earthquake in the last 150 years in New Zealand was the result of the $M=8+$ onshore rupture of the dextral reverse Wairarapa Fault in southern North Island, with ~16 m of displacement [Little *et al.*, 2009].

[25] Wallace *et al.* [2004], using the method of McCaffrey *et al.* [2000] and McCaffrey [2002, 2005], adopted a multiblock model for North Island, where the plate-boundary zone is treated in terms of four to eight long-term rigid but rotating blocks, resting on the subducted plate and undergoing relative slip with variable “coupling factors.” Such a model is the logical extension of the Savage [1983] back slip model, but this time back slip is calculated for all the individual block boundaries, which are assumed to have a steady state slip given by the long-term block motions, over thousands to tens of thousands of years. A key assumption here is that individual block boundaries are likely to be associated with a geodetic signal—i.e., increased gradients in velocity—caused by creep on the fault at depth (see section 9.4), giving the blocks a “geodetic” identity. Thus, the simple campaign GPS profile analyzed by Darby and Beavan [2001] requires at least 15 adjustable parameters to fit the same velocity field, including a knowledge of the geometry and long-term slip rates on the surface faults and coupling factors at depth beneath each block boundary.

[26] Wallace *et al.* [2007] extended the block model to the plate-boundary zone in South Island, defining 9–10 blocks, including block boundaries extending offshore on the eastern side of South Island. Subsequently, several smaller blocks, on a scale of a few tens of kilometers, were introduced in the northern part of South Island [Wallace *et al.*, 2012a]. Some of these block boundaries do not coincide with well-documented mapped surface faults, but are more generalized zones of deformation. The full model for South and North Islands required at least 200 adjustable parameters to model the GPS velocity field, including variable coupling factors both along strike and downdip of major faults or fault zones.

[27] The block models are capable of reproducing the observed horizontal GPS velocity field, with a misfit comparable to the uncertainties in the observed velocities—in fact, this may not be surprising, given the huge number of adjustable parameters. Thus, they potentially provide a framework in which to assess the long-term estimates of major fault slip vectors, over thousands of years. So far, no attempt has been made to fit the block models to the vertical velocity field, so it is unclear whether they are also capable of matching this.

[28] In our view, the multiblock models are unsatisfactory: They provide little insight into the dynamical controls of deformation, the blocks are specified *a priori*, and the elastic deformation is essentially treated as a process that distributes the longer-term deformation rather than the driver of this deformation. The models also combine velocity fields on vastly different time scales, and they deepen the “back slip paradox” because a knowledge of complicated intersecting, but nonslipping, fault geometries is required to determine the elastic velocity field. In particular, where the plate interface is locked, it is unclear how there could be any information in the interseismic velocity field about the partitioning of deformation between local fault slip vectors and block rotation.

3.5. Distributed Ductile Deformation Versus Slip on a Buried Fault

[29] Prescott and Nur [1981] showed that uniform ductile shear at depth can be modeled with slip on buried dislocations—in other words, a simple back slip dislocation model with locked faults near the surface can always be found that looks like a uniformly distributed shear beneath an elastic

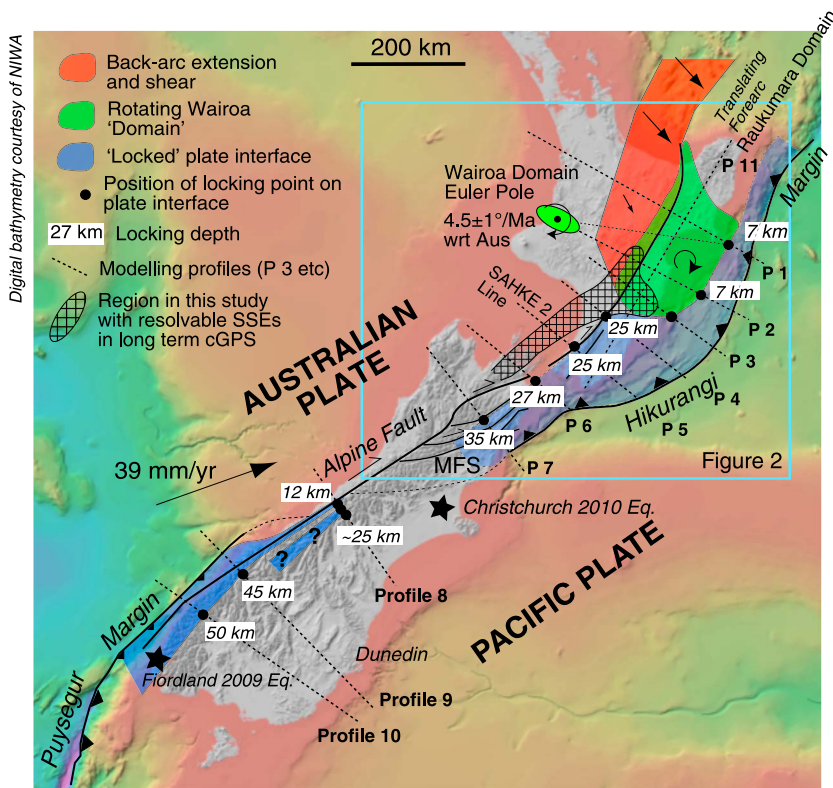


Figure 6. Map of the New Zealand plate-boundary zone, showing offshore bathymetry and onshore shaded relief (courtesy of NIWA) (colored coded from deepest in light blue and shallowest in pink). Here there is dextral oblique convergence of the Pacific and Australian plates, with subduction of Pacific plate in the north along the Hikurangi margin, continental collision in the central part along the Alpine Fault and southern Alps, and subduction of Australian plate in the south along the Puysegur margin. A series of major dextral strike-slip faults, referred to as the Marlborough Fault System (MFS), links deformation in the Hikurangi margin to that in the southern Alps. Stars show epicenters of the Fiordland 2009 and Christchurch 2010 earthquakes. Dashed lines show profiles of cGPS sites analyzed in this study (labeled P1–P7, P11, and Profile 8–10). Long-term cGPS velocities are modeled in this study in terms of (1) free slip on the plate interface (either subduction megathrust or continental fault) at depths deeper than the locking point (best fit defined by black dots with depth) and locked portions of the plate interface (best fit portions are shaded blue); (2) portions of plate interface (cross-hatch shading) where slow slip earthquakes (SSEs) have been resolved; (3) extent and rotation pole (best fit pole shown relative to Australian plate) of the rotating Wairoa domain (shaded green); (4) region of behind arc extension and shear in the Central Volcanic Region and Taupo Volcanic Zone (shaded red); and (5) region north of the Wairoa Domain, referred to as the Raukumara Domain, where the fore arc is translating relative to the Australian plate. Box shows location of Figure 2.

layer. Moore *et al.* [2002] attempted to extend this result to nonuniform shear at depth. The problem is that an elastic strain rate requires an *increase* in elastic stresses over time, whereas stresses do not change with time for steady state ductile strain rates. Thus, there can only be a close link between true ductile and elastic deformation, if elastic stresses are close to zero, so that elastic straining is dominated by the underlying ductile stresses [Savage, 2000]. However, the possibility remains that the deeper parts of the lithosphere are viscoelastic, so that short-term elastic strains eventually become permanent.

[30] In this study, although we focus on searching for a dislocation model of deep slip on the plate interface, we acknowledge that in some cases—particularly beneath New Zealand's Southern Alps—there may be an equivalent ductile flow model (see section 7.3.2). The best way to distinguish between these models is to look for independent evidence of buried slip on a single fault. In much of the New

Zealand plate-boundary zone, the presence of the subducted plate, with a plate interface at the depth required by the dislocation model, is strong evidence for this. The fundamental problem remains calculating the distortion in the elastic layer above this buried slip.

4. A Modified Back Slip Theory for the Elastic Velocity Field Above a Buried Slipping Fault

[31] Key to the back slip method is the existence of a long-term steady state solution to which the back slip elastic distortion can be added (Figure 3). However, it is not generally appreciated that for nonplanar faults, or complex geometries of locked intersecting faults, there is no obvious steady state solution, because slip here requires internal deformation of the rocks away from the faults. In addition, the relative plate-boundary conditions for vertical motion are generally not

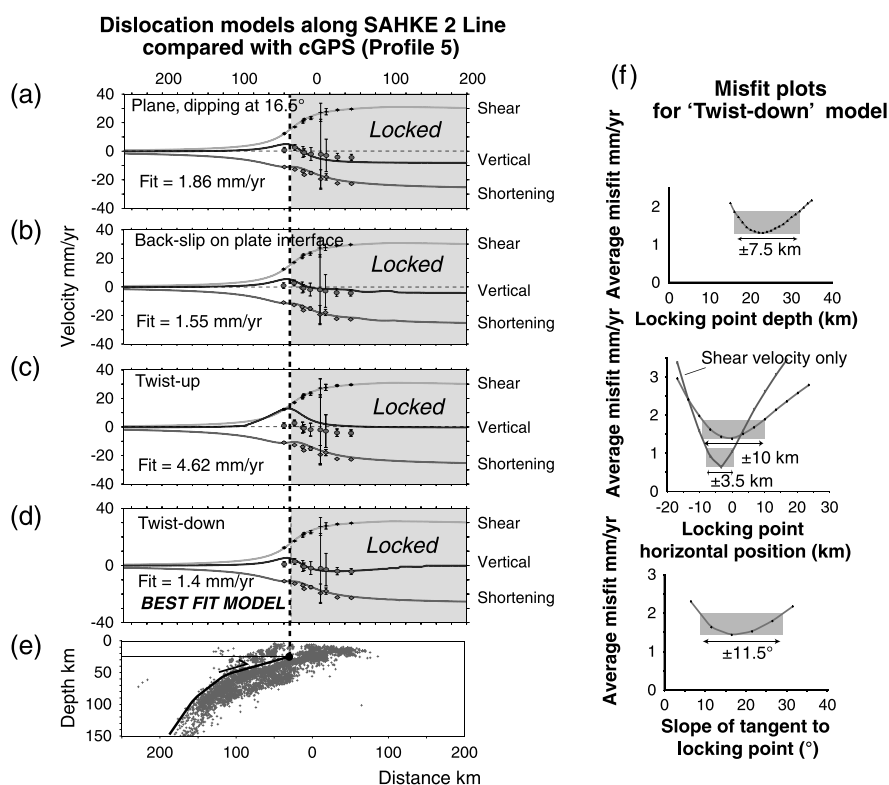


Figure 7. Simple 2-D back slip dislocation models in the southern Hikurangi subducting margin along the SAHKE 2 seismic refraction/reflection line essentially at right angles (azimuth of 128°) to the trend of the subducted plate (Figures 2 and 6, Profile 5). Here the geometry of the plate interface is well imaged by both refractions/reflections (Brook Tozer, unpublished MSc thesis, 2012) and microseismicity (Figure 7e, Geonet earthquake catalogue 2011). In all models, there is a single locking point on the plate interface, which dips at 16.5° in the vicinity of the locking point (i.e., the number of adjustable parameters = 1). The models are compared with all three velocity components of long-term cGPS data in a 25 km swath either side of the profile: (a) back slip on a planar virtual fault; (b) conventional back slip on a virtual fault which is the plate interface up-dip of the locking point; (c) back slip on a concave cylindrical virtual fault, which is horizontal at a depth of 35 km (twist-up model); and (d) back slip on a convex cylindrical virtual fault which is horizontal at the surface (twist-down model). In all cases, the fit to the horizontal velocities is good ($< 1.5 \text{ mm/yr}$), and so the main discriminator between models is the fit to vertical velocities. Note that the planar and conventional back slip models do not satisfy the requirement of no relative plate vertical velocity. The twist-down model (Figure 7d) shows the best fit. (f) Misfit plots for the fit for the twist-down model (Figure 7d), for locking point depth, horizontal position, and slope. Fit is most sensitive to horizontal position, and the fit to the shear component is independent of the model used, providing a powerful constraint on the locking point.

satisfied, resulting in one plate moving vertically up or down relative to the other. These issues are tackled by *Kanda and Simons* [2010] with a model for interseismic deformation that incorporates flexure of the bounding blocks, requiring two additional flexural parameters. We explore below a much simpler model that shares some features with that of *Kanda and Simons* [2010].

4.1. Twist Model

[32] In our view, the difficulty with the back slip analysis is the assumption that the virtual fault must have the same geometry as the nonslipping parts of real faults in the region. There are, in fact, only three general virtual fault geometries that have a steady state solution: planar and convex or concave cylindrical (Figure 4). The last two accommodate a twist about a horizontal axis between the two blocks. The twist may be in the upper plate (a twist-up) or in the lower plate (a twist-down) or a combination of both. A twist-down has a steady state

surface solution with zero vertical motion, whereas a twist-up requires a steady state linear tilt about the point where the virtual fault at depth becomes horizontal.

[33] The elastic solution for either of the twist cases is calculated by treating the virtual fault as a perfect cylinder, which is tangential to the slipping fault at depth just downdip of the locking point. For a twist-down, the unique cylindrical virtual fault is found for which the tangent is horizontal at the surface (Figure 4). For a twist-up, it is necessary to specify the depth of the cylindrical virtual fault where the tangent would be horizontal (Figure 4)—we use a nominal depth of 35 km, coinciding with a typical maximum depth of crustal seismicity, but depths up to 30 km deeper have a relatively small effect on the elastic solution.

[34] The elastic effect of a twist is equivalent to a pure torque exerted between the plates. We note that the response of a uniform elastic beam to a constant bending moment or torque is to bend in the arc of a circle.

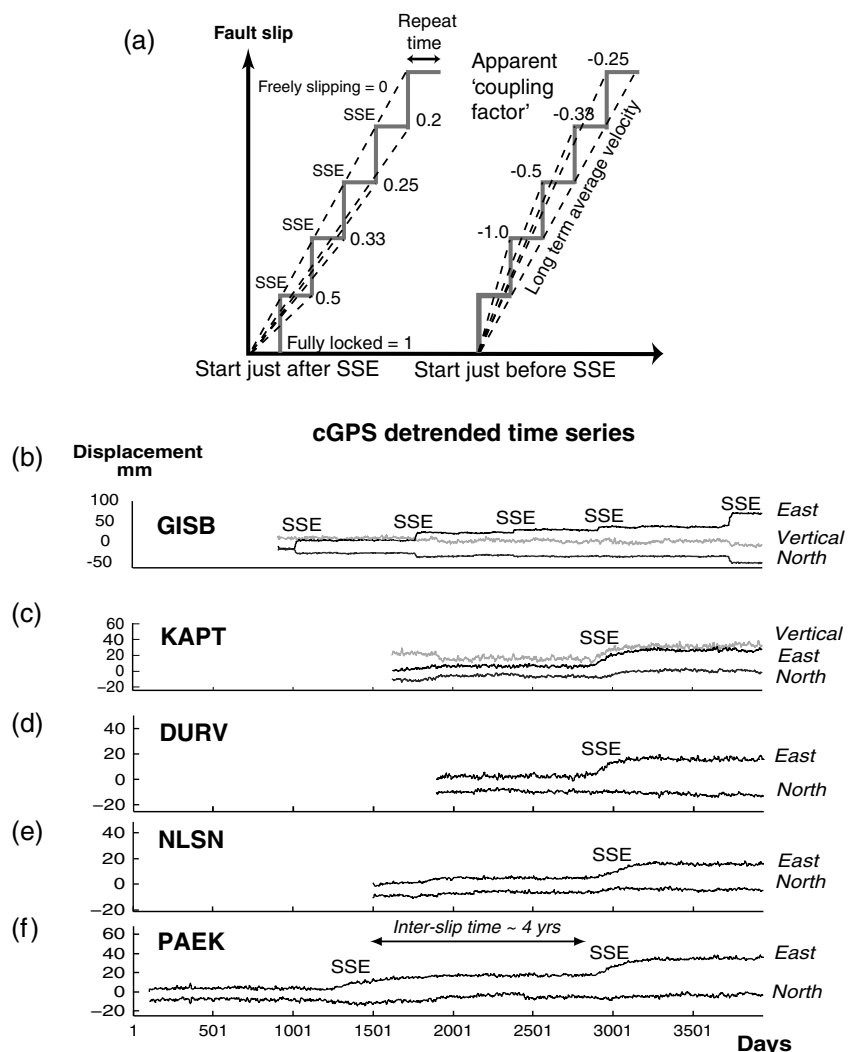


Figure 8. Diagrams illustrating the effect of individual slow slip events (SSEs) over days, weeks, or months, on the long-term cGPS time series and how this can be taken into account in the dislocation models. (a) Plots illustrating a characteristic SSE cycle which fully accommodates fault slip. Two cases are considered, where the time series either starts just after a SSE or just before a SSE. The average velocity for a cGPS time series, determined by the best linear fit, depends on the duration of the time series, the repeat time of SSEs, and when the time series starts in the cycle. Thus, SSE will appear from a geodetic point of view as a partial slip on the fault, defined in terms of an “apparent coupling factor” (1—partial slip). The apparent coupling factor is positive if inter-SSE periods dominate the time series, and negative if SSEs dominate, but is always < 0.5 . (b) Detrended cGPS time series at Gisborne (Table 1, GISB), in the northern part of the Hikurangi Margin, shows many SSEs, every 18 months or so resulting in a very small negative (> -0.2) apparent coupling factor. (c–f) Detrended cGPS time series (Table 1, KAPT, DURV, NLSN, PAEK), in the southern part of the Hikurangi Margin. KAPT, DURV, and NLSN show one SSE, resulting in a significant positive (0.2–0.4) apparent coupling factor, given the interslip time of SSEs shown in the longer time series at PAEK.

4.1.1. Full Velocity Solution

[35] We hypothesize that the full velocity solution at the surface for elastic distortion above a freely slipping buried fault can be treated as a linear combination of the three elastic velocity solutions which have steady states: (1) slip on a planar fault ($V[\text{planar}]$); (2) a twist-up ($V[\text{twist-up}]$), and (3) a twist-down ($V[\text{twist-down}]$). We refer to this as the twist model:

$$V = aV[\text{planar}] + bV[\text{twist-up}] + cV[\text{twist-down}], \quad (1)$$

where $a+b+c=1$ in order to satisfy the plate-boundary

conditions for both the *horizontal* and *vertical* components of motion (note that the relative vertical motion between the bounding plates is zero). In essence, the sum of the three velocity solutions represents the combination of forces and torques that are transmitted across the plate boundary in the elastic layer. In this case, if relative plate motion during the interseismic period is accommodated at depth by free slip on a single fault, such as the megathrust in a subduction zone, then the planar slip contribution ($V[\text{planar}]$) must be zero ($a=0$), because otherwise this would result in relative vertical motion between the bounding plates.

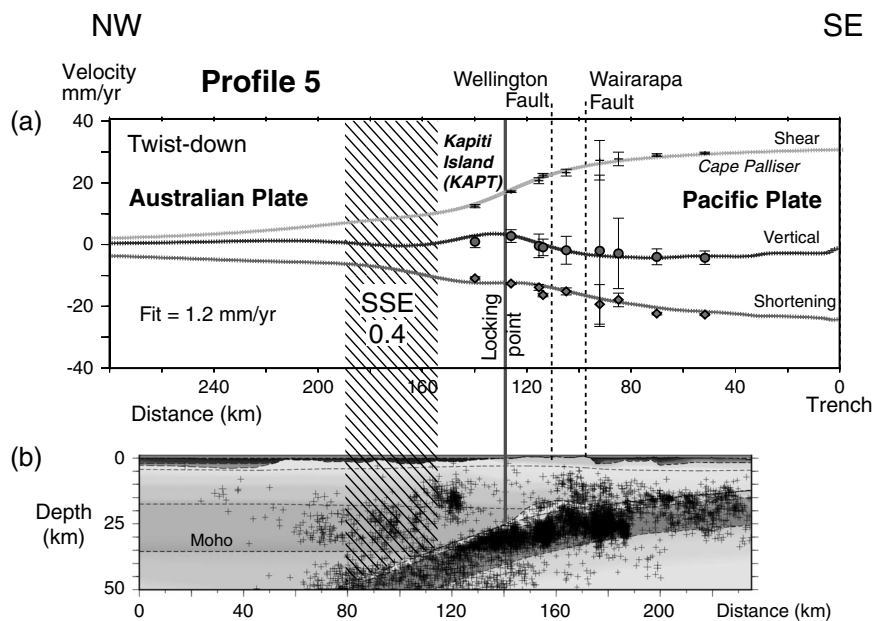


Figure 9. Dislocation model in the southern part of the Hikurangi margin, along the SAHKE 2 seismic refraction/reflection line (Figures 2, 6, and 9b, Profile 5). Note that the depth of the Moho is only constrained close to the plate interface. The misfit for the vertical velocity at Kapiti Island (site KAPT), apparent in the simple single locking point models (Figures 7a–7d), can be accounted for by SSE downdip of the locking point, where the plate interface (subduction megathrust) is at depths of 30–55 km, with an apparent coupling factor of ~0.4. This increases the number of adjustable parameters to four, but reduces the fit here to 1.2 mm/yr, and is consistent with the single SSE observed in Kapiti cGPS time series (see Figure 8c). Note that in Figure 9b, the main locking point coincides with the downdip termination of a low velocity “bump” on the plate interface, which may be accreted sediments (Tozer, unpublished thesis, 2012), and the SSEs are located where the subduction megathrust cuts into the mantle of the overlying Australian plate.

[36] Our analysis shows that in the New Zealand plate-boundary zone, either twist-up or twist-down dominates the interseismic deformation, so that effectively only one of b and c is nonzero.

4.1.2. Local Bending Strains

[37] Although the twist model, described above, satisfies all the plate-boundary conditions, there will be an associated edge effect in the steady state solution where plate motion changes from horizontal translation to a twist (Figure 4), requiring extensional or compression strains at depth. In subduction zones, this is likely to be negligible, because a typical radius of curvature is in the range 500–1000 km, whereas the elastic layer in the subducting oceanic plate will be <50 km. Thus, compressional elastic strain rates at the base of the elastic layer, accommodating bending, will be less than ~5% the surface shortening strain rate. In the New Zealand plate-boundary zone, this is equivalent to ~1 mm/yr at depths of several tens of kilometers, which is essentially undetectable in the surface velocity field. Note that similar edge effects are treated explicitly in *Kanda and Simons* [2010] flexural model for interseismic deformation.

4.2. Modeling in 2-D Versus 3-D

[38] Two-dimensional modeling of the elastic distortion of a slipping buried fault assumes that the nature of the fault (geometry and slip vector) does not change in the direction out of the plane of the modeled section. The analysis treats the fault as a dislocation. M. Henderson (Velocity field of the South Island of New Zealand derived from GPS and

terrestrial measurements, unpublished thesis, University of Otago, 397p, 2003) showed that for slip on a dislocation extending along strike for an infinite distance, the elastic equations simplify, becoming purely kinematic with no dynamical parameters. If the dislocation is of finite length along strike, it will have a lateral edge. The extreme case of the breakdown of the 2-D assumption is when the plane of the modeled profile is close to this “edge.” In fact, it is easy to show that the local elastic velocity field only “sees” the effect of buried slip within a horizontal distance up to twice the locking depth, and so only profiles within this distance of the dislocation edge are significantly perturbed by the presence of the edge.

[39] This is illustrated in Figure 5 for a locking depth of ~25 km, typical of the southern part of the Hikurangi Margin. Thus, the 2-D approximation is a very good representation of the actual elastic distortion, capturing >90% of the velocity field, as long as the nature and geometry of buried faulting is more or less constant on a 50 km horizontal scale perpendicular to the line of the traverse. This holds good for much of the New Zealand plate-boundary, including even the marked lateral shift in the position of the locking point in the central part of the Hikurangi Margin.

4.3. Vertical Motion

[40] Short-term vertical surface velocities, constrained by either continuous GPS measurements, or tiltmeters and tidal gauges, have been used in a wide range of plate-boundary zones to constrain dislocation models of buried fault slip.

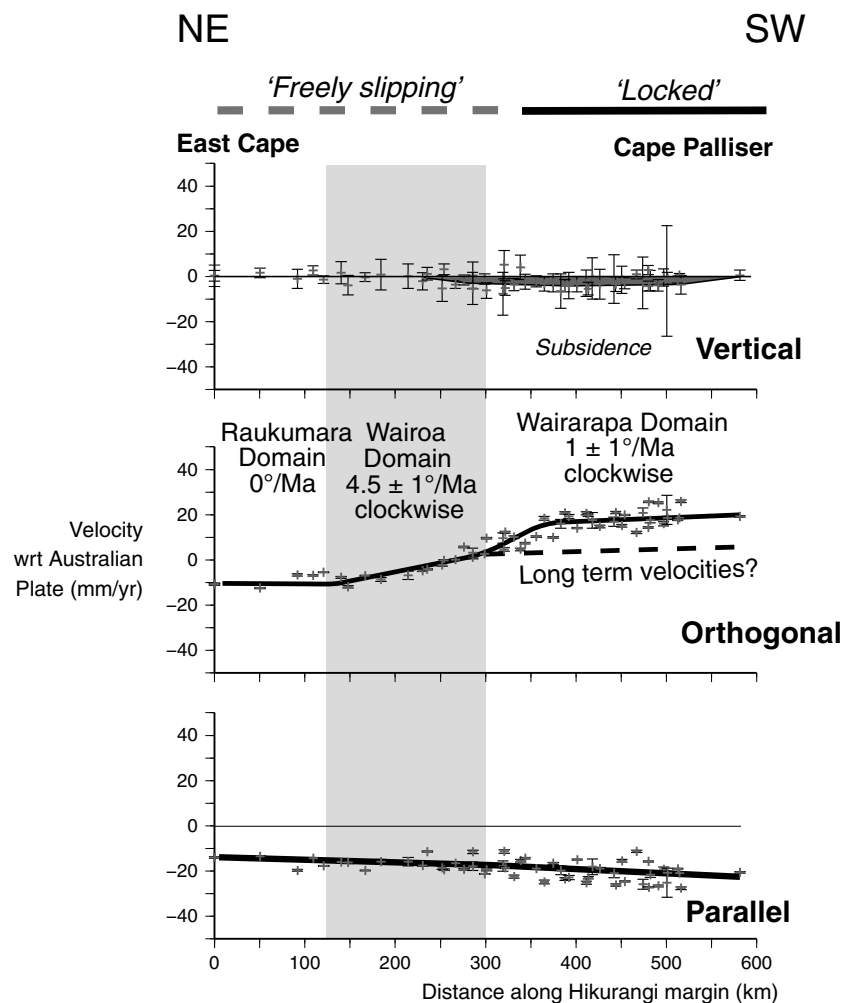


Figure 10. Profile of components of long-term cGPS velocities along the length of the Hikurangi margin (Profile 11 in Figure 6). If the shear velocities are interpreted as a vertical-axis rigid body clockwise rotation with respect to the Australian plate, then there is a remarkable correlation with the rotation domains documented by palaeomagnetic studies for the last ~ 5 Ma, with negligible rotation in the Raukumara domain, rapid clockwise rotation ($4.5^\circ/\text{Ma}$) in the Wairoa domain, and slow clockwise rotation ($<2^\circ/\text{Ma}$) in the Wairarapa domain. However, at the southern end of the profile, where the profile is in the region where the plate interface is locked during the interseismic period, the cGPS contains no information about long-term rigid body rotations. Dashed line here shows hypothetical long-term velocities, consistent with the paleomagnetic data. Farther north, above the freely slipping parts of the subduction interface, the rotations are consistent with those required to model the cGPS velocities in profiles orthogonal to the margin (Figures 2, 6, 12, and 13, Profiles 1–3).

These velocities are generally in the range 1–5 mm/yr and fit the dislocation models surprisingly well (see further on), especially given that other processes could also have a large effect on the long-term vertical tectonics, such as isostatic compensation, erosion and sedimentation, lower crustal flow, and mantle processes. *Vergne et al.* [2001], using a full finite element model for deformation associated with slip on the Main Himalayan Thrust, taking account of all these other processes, concluded that they tend to either have a very small signal <1 mm/yr, or more or less cancel each other out. This may not be true soon after a major earthquake where ductile processes of lithospheric relaxation could have a large effect. However, once this relaxation process has decayed away, the local uncompensated vertical elastic strains seem to dominate the interseismic vertical motions. Over many seismic cycles, the long-term vertical motion will be a combination of the

interseismic, coseismic, and coseismic relaxations, and each will be different.

[41] In this study, we model the cGPS vertical velocities using the vertical elastic displacements predicted in the dislocation models, and we assume that the combined effect of other mechanisms of vertical motion, such as isostatic compensation, erosion, and sedimentation, and crustal and mantle flow, plays a minor role on this time scale. We note that there is no obvious tradeoff between the horizontal and vertical velocities that could result in a good fit to both velocities if this were not the case.

5. Testing the Twist Model

[42] We can assess the fit for various elastic dislocation models discussed in sections 3 and 4, using the cGPS data in

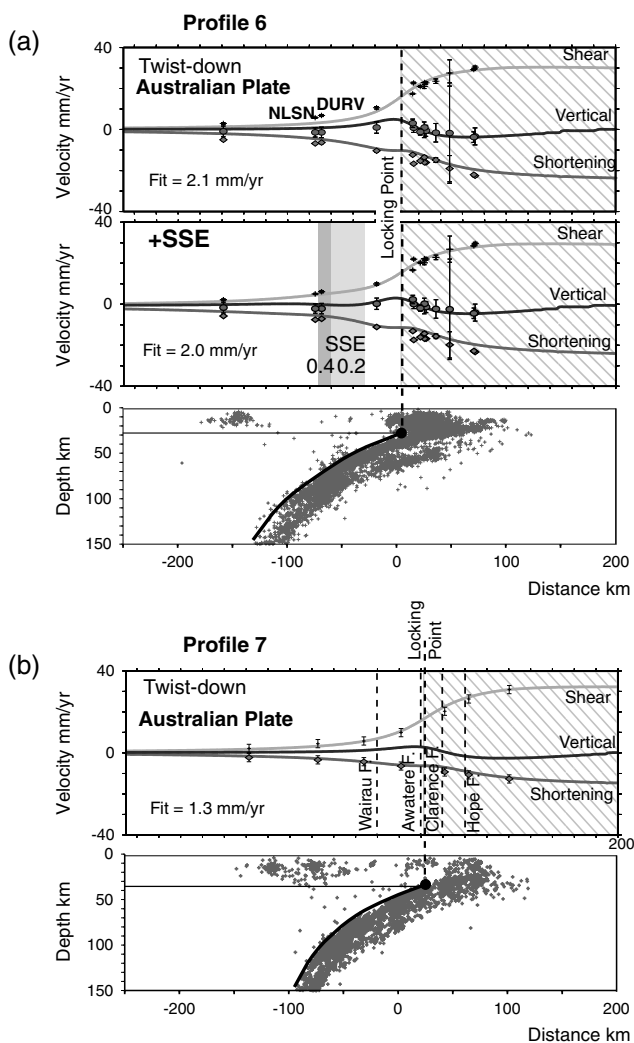


Figure 11. Twist-down dislocation models for the southern Hikurangi margin (Figures 2 and 6) in the vicinity of (a) Profile 6 (Cook Strait) and (b) Profile 7 (Marlborough), showing the geometry of the plate interface (subduction megathrust) from the last decade of microseismicity (Geonet catalogue). Note the very good fit ($\text{fit} = 1.3 \text{ mm/yr}$) in Figure 11b for a single locking depth of 35 km on the subduction megathrust (i.e., the number of adjustable parameters = 1), where the profile crosses all the major Marlborough Faults. This is strong evidence that surface faults do not exist in the interseismic period. In the Cook Strait Profile, the horizontal shear velocities are 2–3 mm/yr too high west of the locking point (Table 1, sites DURV and NLSN). However, incorporating SSEs events here, with an apparent coupling factor of 0.2–0.4, significantly improves the fit (here, the number of adjustable parameters = 6). These apparent coupling factors are consistent with the cGPS time series for the most affected sites NLSN and DURV (Table 1), which are very similar to Kapiti Island (site KAPT, Figure 9), with only one SSE (Figures 8d and 8e).

the southern part of North Island, along the SAHKE 2 deep refraction/reflection line (Figures 2 and 6, Profile 5). This is close to the profile analyzed by *Darby and Beavan* [2001], using ~10 years of campaign GPS data. Here the plate interface is well imaged (B. Tozer, Crustal structure of Wanganui

Basin: Implications for back-arc basin formation, unpublished thesis, VUW, 2012), and there is also a dense network (~20 km spacing) of continuous GPS sites, spanning 4–10 years. For the purposes of this illustration, we use a 2-D model for the traverse trending 128° , essentially perpendicular to the depth contours of the subducted plate. The cGPS velocities are projected on to the profile within a swath 25 km either side.

5.1. Single Locking Point Models

[43] The horizontal and vertical components of velocity are modeled with the simple constraint of a single locking point on the plate interface: downdip of the locking point, the fault is slipping freely at the relative plate motion (calculated at the surface projection of the locking point itself), whereas up dip, it is fully locked and accumulating elastic strain/stress. Thus, there is only one adjustable parameter, given that the geometry of the plate interface is known (e.g., from microseismicity in a Benioff zone).

5.1.1. Dislocation Models

[44] We consider four main models (Figure 7): (i) slip on a planar fault (Figure 7a) that is tangential to the plate interface at the locking point (i.e., a virtual fault that is the planar up dip extension of the slipping fault); (ii) the “classical” back slip method (Figure 7b), where the virtual fault is the plate interface up dip of the locking point; (iii) a pure “twist-up” (Figure 7c) for a virtual fault that is a segment of a circle (in cross section) tangential to the plate interface at the locking point, and subhorizontal at a depth of 35 km; and (iv) a pure “twist-down” (Figure 7d) for a virtual fault that is a segment of a circle tangential to the locking point at the plate interface and horizontal at the surface.

[45] The elastic velocity field for the back slip is calculated using the Okada formulation [Okada, 1985, 1992] of the elastic equations, programmed in Fortran, for the midsection of a dislocation with the characteristic ~600 km length of the Hikurangi Margin. We define a “fit,” which is the root mean square misfit between the three model velocity components and the three components of the data.

5.1.2. Model Results

[46] Figures 7a–7d show that the shear component is identical in all models. This is because in any type of 2-D back slip model, this component is independent of the dip or geometry of the virtual fault [Kanda and Simons, 2012]. Importantly, the shear component shows 180° rotational symmetry about the midpoint, which also coincides with the horizontal position of the locking point. Thus, the shear component can be used to identify the locking point independently of the details of the fault model.

[47] The shortening component is weakly dependant on the geometry of the virtual fault in cases where the fault dip is $<20^\circ$. In marked contrast, the vertical component is sensitive to the geometry of the virtual fault and is therefore the main discriminator between the various models. As discussed in section 4, neither the planar nor classical back slip model satisfy the far field vertical boundary conditions, as they require relative vertical motion of the two plates in the range 4–8 mm/yr. Despite this, the classical back slip model provides a good fit to the observed cGPS velocity components in the onshore part of the plate-boundary zone (average misfit ~1.55 mm/yr). The “twist-up” model satisfies the far-field vertical motion boundary conditions, but fits poorly with the observed vertical velocities.

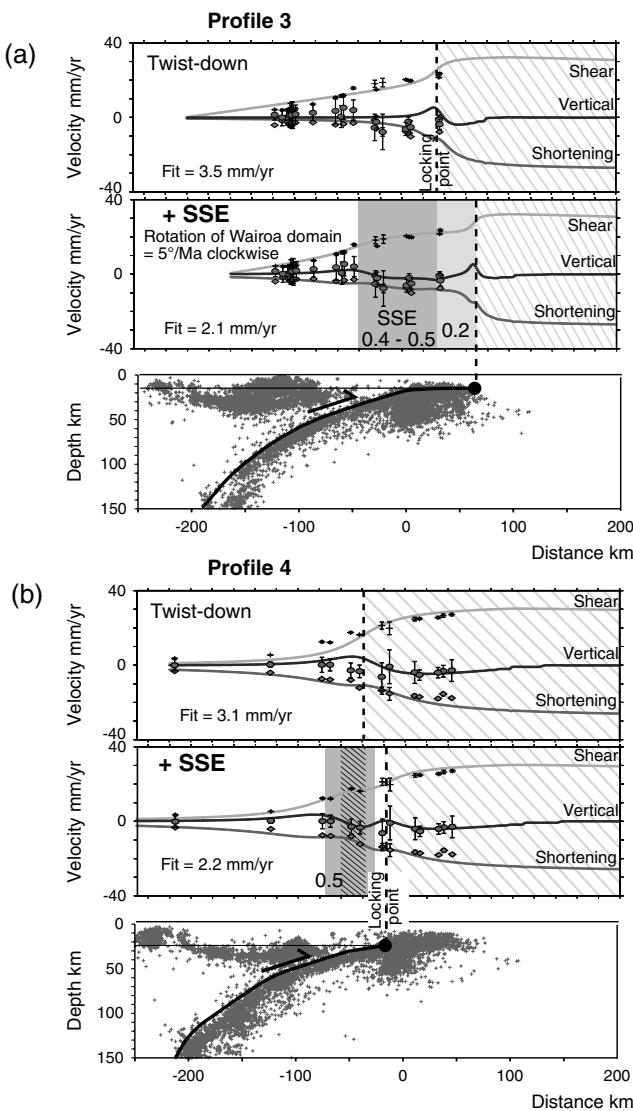


Figure 12. Twist-down dislocation models for the central Hikurangi margin (Figures 2 and 6) in the vicinity of (a) Profile 3 and (b) Profile 4, showing the geometry of the plate interface (subduction megathrust) from the last decade of microseismicity (Geonet catalogue). Top panels for both Figures 12a and 12b show model fit with a single locking point (i.e., the number of adjustable parameters = 1). However, these profiles straddle the southern end of the rotating Wairoa domain (defined in Figure 6). Thus, in Figure 12a, a good fit requires both rotation of the Wairoa domain ($5^{\circ}/\text{Ma}$ clockwise relative to the Australian plate), and a wide region of SSEs, with apparent coupling factors of 0.2–0.5 (i.e., number of adjustable parameters = 5, with rotation parameters of Wairoa domain determined from fits for Profiles 1 and 2 (see Figure 13)). However, in Figure 12b, rotation of the Wairoa domain is not required to model the cGPS velocities, but the fit is significantly improved over a single locking point model by incorporating a wide region of SSEs on the subduction megathrust, with apparent coupling factors of 0.5 or 1 (i.e., number of adjustable parameters = 8). Note that oblique ruling overlay to apparent partial coupling indicates full locked.

[48] In contrast, the “twist-down” model both satisfies both the horizontal and vertical velocity plate-boundary conditions and gives the best fit (average misfit $\sim 1.42 \text{ mm/yr}$) for all three velocity components (Figures 8d and 8e), indicating that in this part of the Hikurangi subduction zone, elastic deformation is dominated by a twist-down between the two plates. We therefore suggest that the relatively good fit of the classical back slip method here stems from the fact that the plate interface close to the locking point approximates an arc of a circle, and so the “back slip” on the locked portion is nearly equivalent to a twist-down.

[49] Finally, the good fit in our model provides strong support for our basic assumption that each individual surface fault in the plate-boundary zone does *not* have a unique geodetic expression caused by buried creep, but rather the elastic layer only responds to the deep steady slip on the plate interface itself (see discussion in section 9.4). In other words, as first pointed out by *Walcott* [1984], based on nearly a hundred years of re-triangulation data in the New Zealand plate-boundary zone, surface faults do not “exist” during the interseismic period.

5.2. Modeling Long-Term Effects of SSEs

[50] A common feature of all the models considered in the previous section (section 5.1) is the failure to model the westernmost vertical velocity at Kapiti Island (Table 1, site KAPT). This area is within a few tens of kilometers of the region where slow slip events (SSEs) have been documented (summarized in *Wallace and Beavan* [2010]).

[51] Slow slip events along the Hikurangi margin appear in the cGPS time series as abrupt shifts in displacement over days to months. They have been located with the assumption that they are slip on the megathrust. Along the western part of the southern Hikurangi margin, they occur where the megathrust is at depths of 30–60 km, and at much shallower depths offshore and much farther east, in the northern part of the Hikurangi margin [*Wallace and Beavan*, 2010, 2012]. We now discuss how to account for the geodetic effects of these events.

5.2.1. SSEs and Apparent Coupling Factors

[52] Many of the cGPS sites closest to the SSE centroids have been in place for periods that are not longer than several SSE repeat times, and the velocities here will be significantly affected by SSEs. The longer the time span of cGPS, the more the effect of SSEs will be averaged out, approximating more nearly to continuous slip. Thus, SSEs will appear from a long-term geodetic point of view as partial slip on the plate interface, with the fraction of partial slip depending on the SSE repeat time, the time scale of GPS measurements, and also when the GPS time series starts in the SSE cycle.

[53] We illustrate two end-member hypothetical relations for a regular SSE cycle, where the slow slip event accommodates the full slip on the fault (Figure 8a). This shows that a diagnostic feature of a SSE in the long-term cGPS record is that it can be characterized by an apparent coupling factor (1—partial slip) that is always ≤ 0.5 for long cGPS time spans, or 1 for very short time spans. Depending on whether interslip periods or slip events dominate (i.e., whether the time series starts just before or after a SSE—see Figure 8a), it will have either a positive or negative value. The Gisborne site is a good example of a small negative apparent coupling with a short interslip period

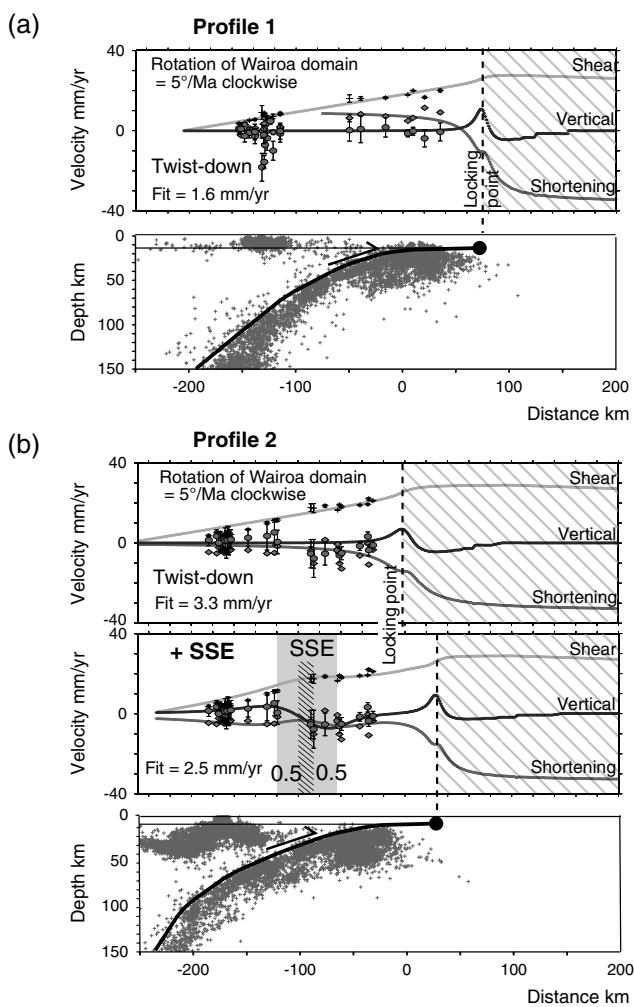


Figure 13. Twist-down dislocation models for the northern Hikurangi margin (Figures 2 and 6) north and south of Hawke Bay: (a) Profile 1 and (b) Profile 2, showing the geometry of the plate interface (subduction megathrust) from the last decade of microseismicity (Geonet catalogue). Note that here the locking point is >50 km offshore, at depths <10 km, and so its precise position is not well resolved. This region is known for frequent SSEs, every 1–2 years [Wallace and Beavan, 2010; Wallace *et al.*, 2012b], but the apparent coupling factors are too low (see text and Figure 8c) for them to be clearly resolved in the long-term cGPS time series. The profiles also cross the rotating Wairoa domain (Figure 6), and this rotation (here modeled at 5°/Ma) is required to model the cGPS velocities. For Figure 13b, the fit, particular to the vertical, is significantly improved over a single locking point model by incorporating a wide region of SSEs on the subduction megathrust, with apparent coupling factors of 0.5 or 1. Note that oblique ruling overlay to apparent partial coupling indicates full locked. A total of 12 adjustable parameters were used for the combined best fits of Profiles 1 and 2 (3 for rotation of Wairoa Domain, and 9 for locking points and partial coupling), fitting >51 data points.

(Figure 8b), and the Kapiti site shows a large positive apparent coupling with a longer interslip period (Figure 8c).

5.2.2. SSEs Along the SAHKE 2 Line (Profile 5)

[54] We can test this simple model in for the SAHKE 2 line (Figures 2 and 6, Profile 5), by searching for an apparent

coupling factor on the slipping part of the plate interface that provides the best fit to the data. We search for a coupling factor that accounts for the relatively low vertical velocity at Kapiti Island (Table 1, site KAPT), on the western limit of the traverse. For this, we calculate the twist-down by using a curved virtual fault that is tangential to the deepest part of the SSE partially locked zone (depth ~55 km), and then add in the relevant partial forward slip along the megathrust up to the long-term locking point at a depth of ~25 km. In practice, this is very similar to using a series of “back slip patches” with a coupling factor <1, although it is the forward slip approach that can be both rigorously justified and gives a slightly better fit to the cGPS observations.

[55] Here we only looking for a solution that illustrates the effect of SSEs—given the sparsity of data, there is a range of possible solutions for this particular profile, and so we choose a solution consistent with parallel profiles with better data coverage (see section 6.2). We can reduce the average misfit of the model to the cGPS velocities, along the SAHKE 2 profile, to ~1.2 mm/yr, if there is a coupling factor of 0.4 for the subduction megathrust at depths between 35 and 50 km, about 40–70 km west of Kapiti Island (Figure 9). Note that this improved fit also requires shifting the long-term locking point about 4 km eastward.

[56] The interslip time for SSEs at any point in the southern part of the Hikurangi Margin is 4–5 years (see Figure 8f, cGPS time series for PAEK) [Wallace and Beavan, 2010]. Thus, a coupling factor of ~0.4 is consistent with the cGPS time series for the Kapiti site (Table 1, KAPT), which shows one major SSE event about midway through the recording period (Figure 8c).

5.2.3. Variable Length cGPS Time Series

[57] The previous analysis of the effect of SSEs, in terms of an apparent partial coupling on the plate interface, assumes that the cGPS time spans for all individual sites are the same. In actual fact, the duration and start of the cGPS time series vary from site to site. However, importantly, only cGPS sites that are located horizontally less than about the locking depth (<50 km) from the horizontal projection of the SSE centroid, have long-term time average velocities that are significantly perturbed by SSEs, and for these sites (mainly the extreme western sites in southern North Island), the time series are similar. This is why the method we use to deal with the effect of SSEs on the long-term velocities works so well (see section 6.2) and has virtually no effect on our estimate of the position of the long-term locking point.

[58] Our method has the added advantage of making it possible to directly locate the region of plate interface prone to SSEs using the long-term GPS velocities rather than by identifying individual events.

5.3. Application of Methods in This Study

[59] The application of methods used in this study is summarized below:

[60] 1. The velocity field reflects driving forces in the plate-boundary zone. The dominance of subduction in the north and south (see section 1.1) suggests that it is free slip on the plate interface in the subduction zone, below some locking depth, which is the main driver of elastic distortion here. In section 7, we extend this idea by considering a single free slipping plate interface at depth beneath the central part of the

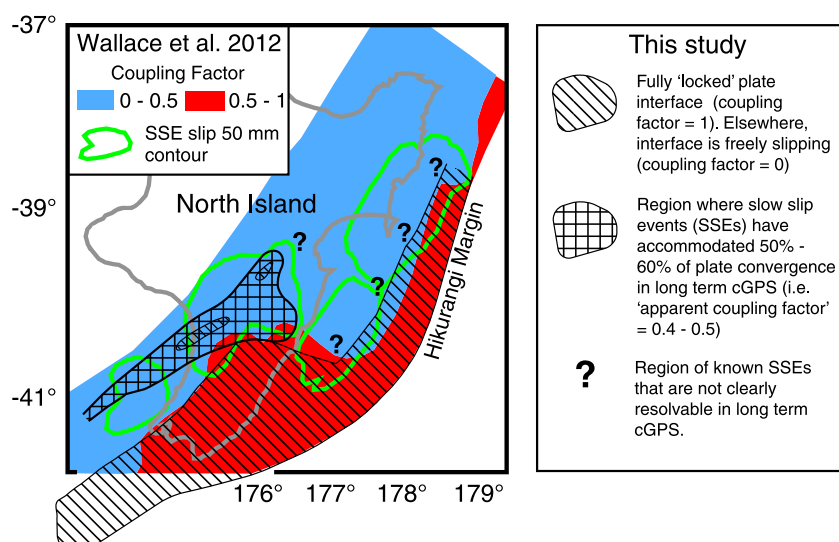


Figure 14. Simplified map of interplate coupling on the Hikurangi margin in North Island and northeastern South Island, after Wallace *et al.* [2012a], with apparent coupling factor from our study, overlaid as oblique ruling (fully locked) or cross-hatch (partial slip). Wallace *et al.*'s model is simplified with a color-coded red (coupling factor 1–0.5) and blue (coupling factor 0–0.5), based on a complex multiblock model of deformation, which combines long-term Holocene slip rates on the boundaries of hypothetical rigid blocks with GPS data.; the coupling factor on faults and the subduction interface are assumed to smoothly vary from 1 to 0, with the greatest gradient close to the 0.5 contour, so that lower coupling factors rapidly approach zero. Our model, with either freely slipping (coupling factor = 0) or fully locked (coupling factor = 1), shows broad similarities with the complex multiblock models, with our fully locked region (coupling factor = 1) more or less coinciding with the region where coupling factor in the multiblock models is in the range 1–0.5. Our study also resolves a region of apparent partial coupling downdip of the locking point line, which coincides with a region of known SSEs with relatively long repeat times. However, SSEs are not clearly resolvable in regions marked with question marks, where SSEs are also known to occur with relatively short repeat times (1–2 years).

plate-boundary, in the region of the Alpine Fault and Southern Alps, as a driver of elastic continental deformation.

[61] 2. Individual surface faults do not have a resolvable expression in the continuous GPS period, so knowledge of their slip rates/geometry is not required to model GPS velocity field within its uncertainties—in effect, we are assuming that they do not “exist” in the interseismic period because there is no localized buried creep in shear zones at depth other than on the plate interface itself. Thus, the model makes no assumptions about the long-term slip rates on these faults, or rotation of the intervening small scale fault blocks, except that over many seismic cycles the combined effect of slip on all the active faults will relieve the buildup in elastic stress/strain. However, in section 6, we require rotation of a wide region in the northern part of the plate-boundary, where back-arc extension has created a fore-arc “microplate” or domain.

[62] 3. We consider average GPS velocities over the full available time span (up to 10 years) in order to minimize the effect of slow slip events.

[63] 4. We use 2-D dislocation models in profiles (Figures 2 and 6, and see section 4.2), so that cGPS velocities are projected on to the profile within a swath 25 km either side, and we use the Okada formulation of elastic distortion associated with slip on a rectangular dipping dislocation [Okada, 1985, 1992], programmed in Fortran. We define a virtual fault to be the circular (in cross section) extension of the freely slipping portion to the surface, tangential to the

freely slipping part close to the locking point (or SSEs), but either horizontal at the surface (a twist-down) or horizontal at some reference depth (a twist-up).

[64] 5. We define a “fit,” which is the root mean square misfit between the model and measured velocity components (three each). This is equivalent to a reduced chi-square parameter, where the standard deviation is taken as 1 mm/yr.

[65] 6. As a first assumption, we only consider slip or no slip on the plate interface—i.e., “coupling factor” = 0 or 1 and the plate interface slips at the Australian/Pacific relative plate motion. In other words, we assume there is no transition zone or edge effect at the boundary between locked and slipping portions of the plate interface. We search for the horizontal location and depth of the locking point or points on the plate interface, along the entire length of the plate-boundary, which gives a fit better than some chosen level. We then seek to improve this fit by adding the effect of SSEs by considering partial forward slip (equivalent to a coupling factor ≤ 0.5 or 1, depending on the time span of the cGPS sites compared with the repeat time of SSEs) downdip of the long-term locking point.

[66] An important caveat is that elastic modeling is inherently nonunique, and so a good fit does not mean that the model represents reality. However, further support comes from showing that freely slipping parts of the plate interface coincide with geophysically imaged lithospheric features (see below).

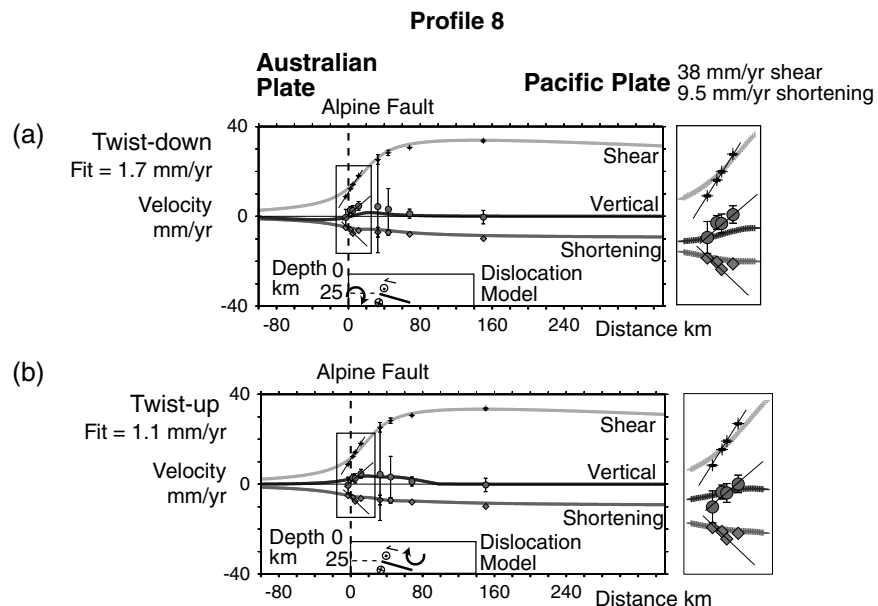


Figure 15. Deep slip dislocations models for the plate-boundary zone in the vicinity of the central Southern Alps (Figure 6, Profile 8). The freely slipping part of the plate interface moves at the relative plate convergence. A single plate interface with a locking depth of 25 km fits the long wavelength pattern of cGPS velocities in the profile, for both (a) twist-down and (b) twist-up models (i.e., number of adjustable parameters for each model = 2). The twist-up model shows a better fit to the vertical velocities. However, neither model matches the spatial gradients of velocities close to the surface outcrop of the Alpine Fault (enlarged in inset boxes).

6. Hikurangi Margin

6.1. Tectonics of the Hikurangi Margin

[67] In the north, the tectonics is dominated by westward subduction of Pacific oceanic lithosphere beneath North Island, along the Hikurangi margin, at the southern end of the Tonga-Kermadec subduction zone. Back-arc extension behind this subduction zone, in the Havre Trough, extends into northern central North Island as the Taupo Volcanic Zone (TVZ), terminating in the vicinity of Ruapehu volcano at 39.3°S (Figures 2 and 6). The volcanic arc does not extend south of Ruapehu, and deformation is dominated by dextral shear along the North Island shear belt, which includes the Mohaka, Wellington, and Wairarapa Faults. Subduction terminates beneath northern South Island, where deformation occurs in a zone of dextral transpression in the Marlborough Fault System (MFS), including the Hope, Clarence, Awatere, and Wairau Faults (Figures 2 and 6).

[68] The Hikurangi margin is an unusual ocean-continent convergent margin. The Hikurangi plateau, one of three pieces of a large igneous province, is currently being subducted all along the east coast of the North Island. Its downdip extent is not fully resolved, but its presence means that the subducting plate is significantly more buoyant than ocean lithosphere of comparable age, and that the crust of the subducting plate is not a normal oceanic crust (summarized in Wallace *et al.* [2009]). Moreover, the Hikurangi margin has no seismological, archeological, or geological evidence of great subduction earthquakes (summarized in Wallace *et al.* [2009]). The largest historical, but preinstrumental, earthquakes was the $M8+$ earthquake on the Wairarapa Fault in 1855. This produced ~16 m of dextral surface displacement [Little *et al.*, 2009] and uplifted the region to the west by 1–5

m. Importantly, during the period of cGPS observation, no plate interface event exceeded $M6$. However, the region is prone to pervasive slow slip events (SSEs) with repeat times from 1 to 6 years (see further on).

[69] The geometry of the subducted Pacific plate is well constrained from tens of thousands of microearthquakes, recorded in the Geonet catalogue over the past 30 years (Figures 7 and 9) [Reyners *et al.*, 2011]. The trench lies about 50–100 km offshore, at a depth of 2–4 km. We use the top of the region of deep intense microseismicity in the Benioff zone to define the location of the subduction megathrust. This shows that the plate interface dips at 10°–25° where it is contact with the overlying crust, and the trend of the subduction zone is 10°–15° oblique to east coast of North Island. This way, progressively shallower depth contours underly the east coast toward the south, ranging from ~15 km beneath Gisborne, in northeastern North Island, to ~10 km beneath Cape Palliser in southeastern North Island. The frontal thrust effectively comes onshore in northern South Island, forming the southern edge of the Marlborough Fault System. Here the subducted plate dips more steeply, reaching depths of 30–50 km beneath the Marlborough Fault System.

6.1.1. Wairoa “Domain”

[70] The presence of back-arc extension in northern North Island complicates the plate tectonics of the region, effectively introducing two additional quasi-rigid “microplates,” referred to here as the Wairoa and Raukumara domains (Figures 6 and 10). Paleomagnetic data (summarized in Lamb [2011]) show that the Wairoa domain has rotated about a vertical-axis coherently about 70° clockwise relative to the Australian plate in the last 20 Myr, with 20°–30° clockwise rotation in the last 5 Myr. The northern boundary of the rotating Wairoa domain lies north of Hawke Bay, following an arcuate and diffuse

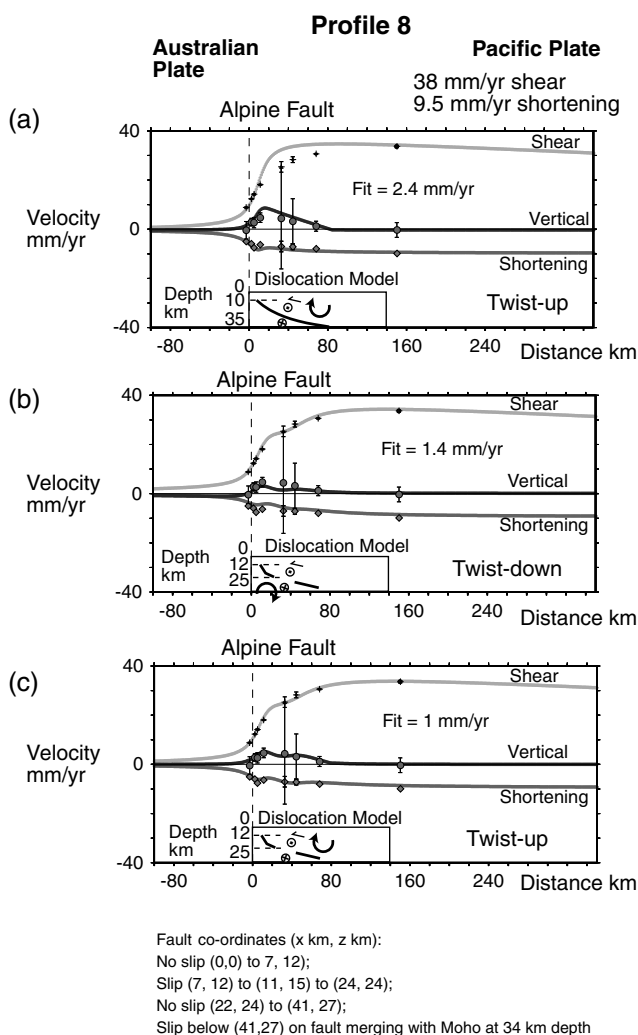


Figure 16. Shallow slip dislocation models for the plate-boundary zone in the vicinity of the central Southern Alps (Figure 6, Profile 8). The freely slipping part of the plate interface moves at the relative plate convergence. (a) Here a single plate interface with a locking depth of 12 km (i.e., number of adjustable parameters = 2) fits the short wavelength pattern of cGPS velocities close to the surface outcrop of the Alpine Fault, for both twist-up (illustrated here) and twist-down, but does not match the long wavelength shear velocities. (b and c) A model that fits the long wavelength shear velocities (for either twist-down or twist-up) involves introducing a locked patch at a depth of ~25 km, at a distance of 25–40 km SE of the Alpine Fault surface trace (i.e., number of adjustable parameters = 8, although reducing this to 6 by removing curvature of shallow freely slipping segment has very little effect on fit). The twist-up model has the best fit with all components of velocities, with a fit of 1 mm/yr.

zone of strike-slip and normal faulting between Gisborne and the Bay of Plenty (Figure 2). Paleomagnetic data show that the region to the north [Lamb, 2011] has not rotated relative to the Australian plate in the last ~24 Ma. This defines the Raukumara domain, which has undergone ~100 km of SE, directed translation during the last ~5 Ma as a consequence of back-arc extension and the opening up of the Havre Trough. The southern boundary of the Wairoa domain lies

south of Hawke Bay, where paleomagnetic data suggest that the Wairarapa domain (Figure 10) has undergone <5° clockwise rotation in the last ~2.5 Ma or <2°/Ma with respect to the Australian plate [Lamb, 2011].

6.1.2. Geodetic Rotation Rates

[71] The pattern of vertical axis rotation along the eastern side of North Island is well resolved in the cGPS data. Figure 10 shows the components of velocity parallel and perpendicular to a profile trending 212°, in a 50 km wide swath extending down the entire length of North Island from Hicks Bay in the north to Cape Palliser in the south (see location in Figures 2 and 6). The component of velocity parallel to the profile is directed southward and shows extension, increasing from 16 mm/yr in the north to 26 mm/yr in the south. The gradient of the component of velocity perpendicular to the profile is consistent with and can be modeled as a vertical axis rotation. In this case, there is a remarkable correlation between the cGPS pattern of rotation (relative to the Australian plate), and the paleomagnetic domains, with a negligible GPS rotation rate (<1°/Ma clockwise) north of Gisborne in the Raukumara domain, and a clockwise rotation of $4.5 \pm 1^\circ/\text{Ma}$ farther south in the Wairoa domain, as far as ~40°S. The southern part of the profile suggests a significantly lower clockwise rotation rate in the range <2°/Ma.

[72] In this study, we do not attempt to model back-arc extension across the TVZ (Figures 2 and 6) but focus on the motion of the Wairoa domain, relative to both the Australian and Pacific plates (see below). Extensional deformation in the TVZ is presumably driven by the buoyancy contrast between the back arc and trench, acting on a thin elastic layer [Lamb, 2006]. We search for the pole of rotation that best fits the cGPS velocities in the Wairoa domain in the context of our elastic modeling.

6.2. Elastic Modeling in 2-D of the Hikurangi Margin

[73] The continuous GPS velocity field is modeled in a series of profiles across the Hikurangi margin (Figures 2 and 6, Profiles 1–7), trending more or less orthogonal to the depth contours of the subducted plate, deduced from the seismogenic Benioff zone. The principal features of the modeled profiles are described below (Figures 9–12):

[74] 1 For profiles in the southern part of the Hikurangi margin (Figure 2, Profiles 4–7; south of Cape Turnagain in North Island at ~40.5°S to Kaikoura in South Island at ~42.5°S), there is a good fit (<2 mm/yr) to a single locking point on the subduction megathrust at depths in the range 25–35 km (Figures 9 and 11). Note that because of the sparsity of cGPS sites in northeastern South Island, we use a published profile of campaign data [Wallace *et al.*, 2007] for the southernmost profile (Figures 1a, 6, and 11b, Profile 7). The main feature is the progressive shallowing of the locking points toward the north. Thus, the horizontal trace of the locking point line, from south to north, follows the Awatere Fault in northeastern South Island at a depth of 35–30 km (Figures 2 and 6, Profiles 6 and 7), crossing Cook Strait slightly inland of the west coast of southernmost North Island at a depth of ~25 km (Figures 2 and 6, Profiles 4 and 5). It then continues at this depth, more or less following the Wellington Fault as far as ~41°S, before swinging abruptly to the east and passing offshore to much shallower depths (15–20 km) in the vicinity of Cape Turnagain at ~40°S (Figures 2, 6, and 12, Profile 3). Farther north,

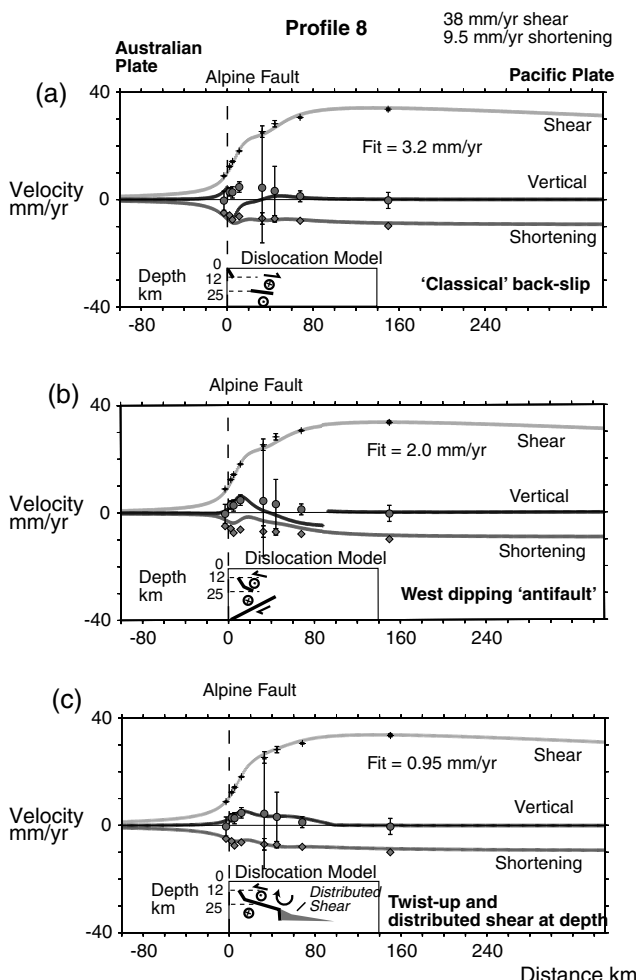


Figure 17. More shallow slip dislocation models for the plate-boundary zone in the vicinity of the central Southern Alps (Figure 6, Profile 8). The freely slipping part of the plate interface moves at the relative plate convergence. (a) This has same geometry as that for the best fit twist-up model, illustrated in Figure 16c, but the velocity field is calculated using the conventional back slip approach, with back slip on the putative nonslipping parts of the plate interface (i.e., number of adjustable parameters = 6). This fails to satisfy the boundary conditions for vertical velocities between the two plates. (b) Here as well as shallow slip, back slip is calculated for an antithetic fault at depth (i.e., number of adjustable parameters = 8). Again this has a poor match with vertical velocities. In addition, the shortening velocities are not well matched. (c) Here we model a zone of distributed shear at depth. The best fit model involves a twist-up, with free slip on a fault deeper than 12 km at 0.75 times the relative plate convergence (i.e., ~29 mm/yr of dextral shear), which passes down into a distributed shear zone at depths >27 km, which accommodates the remaining ~9 mm/yr of dextral shear (i.e., number of adjustable parameters = 7).

precise position is not well resolved, except that it must lie well offshore at shallow depths (Figures 2, 6, and 13, 5–15 km in Profiles 1 and 2).

[75] 2 For all profiles north of where the locking point line swings offshore (Profiles 1–3), the rotation of the Wairoa domain (Figures 6 and 10) is required to explain the

velocities. Here both the shortening and shear components constrain the pole of rotation of the Wairoa microplate, relative to the Australian plate, to lie ~100 km WNW of Ruapehu volcano at ~39°S, with a clockwise rotation rate of $4.5 \pm 1^{\circ}$ /Ma (Figures 2, 6, and 10).

[76] 3 The fit to vertical velocities downdip of the locking point, as well as horizontal velocities in the region where the locking point line swings offshore, is significantly improved by including the effects of slow slip events. The best fit defines an ~40 km wide zone of SSEs on the plate interface, extending parallel to and west of the locking point line, at depths of 35–55 km (Figures 6 and 9–14). These generally are modeled with apparent coupling factors 0.4–0.5, consistent with the occurrence of SSEs in the nearest cGPS time series (for example, sites KAPT, DURV, and NLSN in Table 1 and Figures 8 and 11), but with some localized patches that are fully locked (Figure 14). Slow slip events appear to be particularly marked in a wide region just north of where the locking point line swings abruptly eastward (Figures 6, 12b, and 14).

6.3. Comparison With Previous Studies

[77] We compare here our results with those from multiblock models of the New Zealand plate-boundary zone [Wallace et al., 2004, 2007, 2012a].

6.3.1. Spatial Distribution of "Locked" Plate Interface

[78] The geometry of the locked region derived in this study shows broad similarities with those determined in the multiblock models. In particular, the marked step in the highly coupled parts in the block model closely follows the eastern swing in the locking point line in this study (Figure 14). The key point here is that the much greater complexity of the multiblock models, together with the incorporation of Holocene fault slip rates and block rotation, is not required to recover the main features of the pattern of locking on the plate interface. In addition, there is no need to invoke transition zones with variable partial slip between locked and slipping portions of the plate interface. For example, we can simply model as fully locked extensive portions of the plate interface that require coupling factors in the range 0.5–1 in the multiblock models. Thus, it is possible that some of the details of partial coupling in the multiblock models could be due to trade offs between the details of fault locking and both the geometry of the blocks and their relative motion and are essentially a result of the choice of block geometry and long-term block motion. In other words, the requirement in these models for the blocks to have a distinct geodetic identity may force a solution with partial coupling or free slip at depth on their boundaries.

[79] In our view, partial coupling mainly reflects incomplete averaging of the SSE cycle, and so any model based on different GPS time series or epochs will always give a different picture of partial coupling. In our model, we differentiate between very long term fully locked portions of the plate interface and those parts that have "apparent partial coupling" due to SSEs. We note as well that the multiblock models do not attempt to fit the vertical velocities, which are most sensitive to "apparent partial coupling factors" in the longer-term GPS record [Kanda and Simons, 2012]. For example, apparent partial coupling along Profile 2 in the northern Hikurangi margin is only well resolved in the vertical long-term cGPS velocities (Figure 13b).

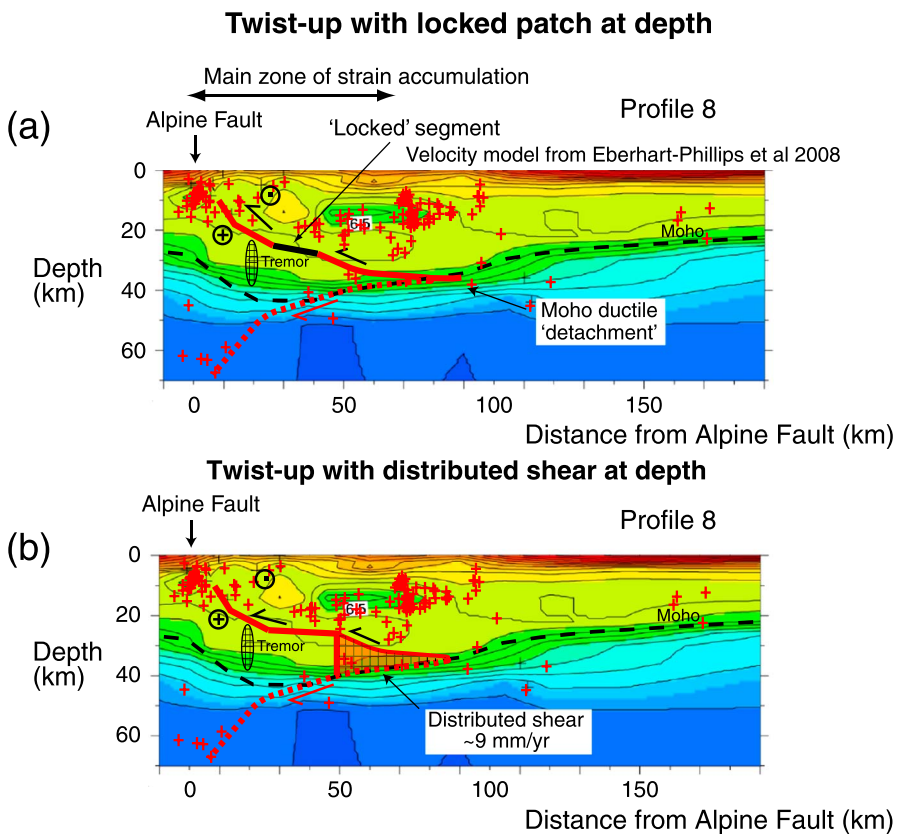


Figure 18. Two alternative preferred best fit models in this study for the central southern Alps (Figures 16c and 17c) compared with the crustal seismic velocity structure from earthquake tomography [from Eberhart-Phillips *et al.*, 2008]. Location of tremor also shown [Wech *et al.*, 2012]. The kinematics here require the Australian plate to extend in cross section up to 100 km beneath Pacific plate. In this case, crustal thickening is principally caused by underthrusting. However, the dominant motion is dextral strike-slip out of the plane of section. (a) Twist-up model with locked patch at ~25 km depth, and freely slipping parts of plate interface moving at full relative plate motion. (b) Alternative model, involving distributed shear at depths >27 km (see Figure 16c) and free slip up to a depth of ~12 km at 0.75 times the plate convergence rate (see text).

6.3.2. Tectonic Rotation of the Hikurangi Margin

[80] The pattern and rate of tectonic rotation along the Hikurangi margin, determined in this study, differ markedly from the results of the multiblock models. Wallace *et al.*'s [2004] multiblock model suggested that the entire length of the Hikurangi margin in North Island, extending for ~400 km, is rotating clockwise at 2–3°/Ma with respect to the Australian plate, about Euler poles located about ~100 km west and offshore of western North Island, in contrast to the pattern and rate suggested by palaeomagnetic data [Lamb, 2011]. Lamb [2011] showed that this conclusion largely stems from the assumption in the multiblock models that the margin consists of a number of very long and thin coherent blocks or slivers, extending for its entire length.

[81] The cGPS data analyzed in this study, both in transects parallel (see section 6.1.2) and perpendicular to the Hikurangi margin (Figures 2 and 6), resolve a pattern of rotation which is consistent with the paleomagnetic data for the freely slipping parts of the margin (section 6.1 and Figure 10). However, we emphasize that the interseismic velocity field alone *cannot* provide information about tectonic rotation in the southern part of the Hikurangi margin, in regions where the plate

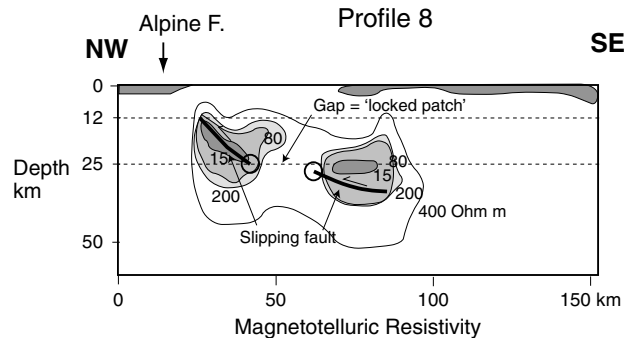


Figure 19. Crustal resistivity model for Southern Alps determined along a profile about 50 km north of Profile 8 from Wannamaker *et al.* [2009], shown as smoothed contours of resistivity in Ohm m. There is a marked zone of low resistivity which correlates with the shallow slipping part of the plate interface in the twist-up dislocation model in this study (Figures 16c and 18). The locked patch in the dislocation model coincides with the high resistivity “gap,” and the downdip slipping zone starts where low resistivity is again observed.

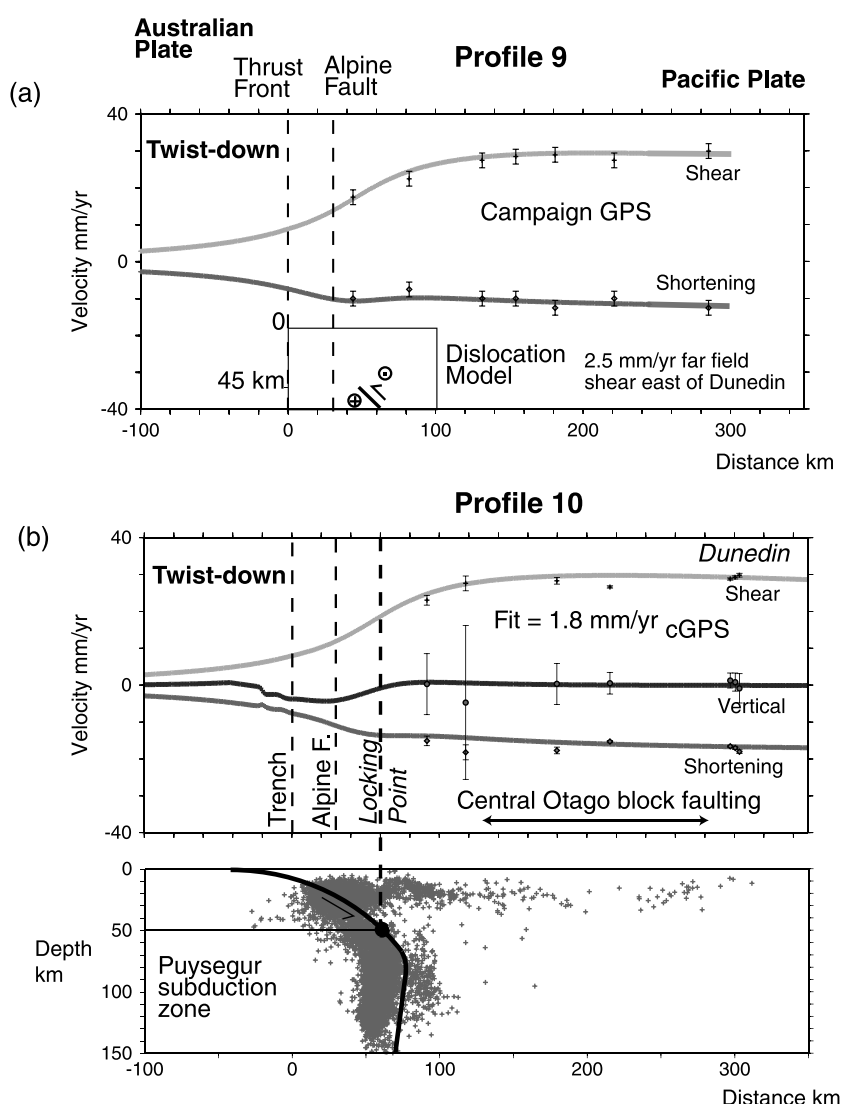


Figure 20. Deep slip dislocation models for the plate-boundary zone in the vicinity of the southern South Island, across the Puysegur subduction zone (Figure 6, Profiles 9 and 10). The freely slipping part of the plate interface moves at the relative plate convergence. A single-plate interface with a locking depth of 45–50 km fits the long wavelength pattern of cGPS velocities in the profile, for a twist-down model. The long wavelength velocity field is determined by a single locking point on the subduction megathrust (i.e., number of adjustable parameters = 1). The good fit to the data shows that there need not be a correlation between local interseismic and finite strain rate, and thus it is not possible to use GPS data to estimate the rate of shortening across block reverse faults in Central Otago. Likewise, the GPS data cannot be used to infer the rate of motion on the Alpine Fault. (a) Single locking point dislocation model for Profile 9 (i.e., number of adjustable parameters = 1), compared with a published campaign data transect [Wallace *et al.*, 2007], because of the dearth of cGPS sites here. There may be a problem with the reference frame for these data, because they require ~2.5 mm/yr of shear with respect to the Pacific plate east of Dunedin [Beavan *et al.*, 2002; Wallace *et al.*, 2007], which is not apparent in over 10 years of cGPS data. (b) Single locking point dislocation model for Profile 10, compared with cGPS data (this study).

interface is locked, although a low rate of rotation (<2° clockwise) is consistent with both the cGPS and palaeomagnetic data (Figure 10) [Lamb, 2011].

7. Oblique Continental Collision

7.1. Tectonics of Oblique Continental Collision

[82] In central South Island, relative plate motion occurs as a ~200 km wide zone of dextral transpression through

continental lithosphere. Dextral shear in the Marlborough Fault System, at the southern end of the Hikurangi subduction zone, is transferred to dextral strike-slip (~38 mm/yr) and thrusting (9–10 mm/yr) parallel and perpendicular to the Alpine Fault (Figure 6). At least 70% of the dextral strike slip (~30 mm/yr) is taken up on the Alpine Fault itself [Norris and Cooper, 2001], which has a total displacement of ~500 km in the last ~20 Myr. The small component of active convergence, orthogonal to the Alpine Fault, is resulting in rapid uplift of the

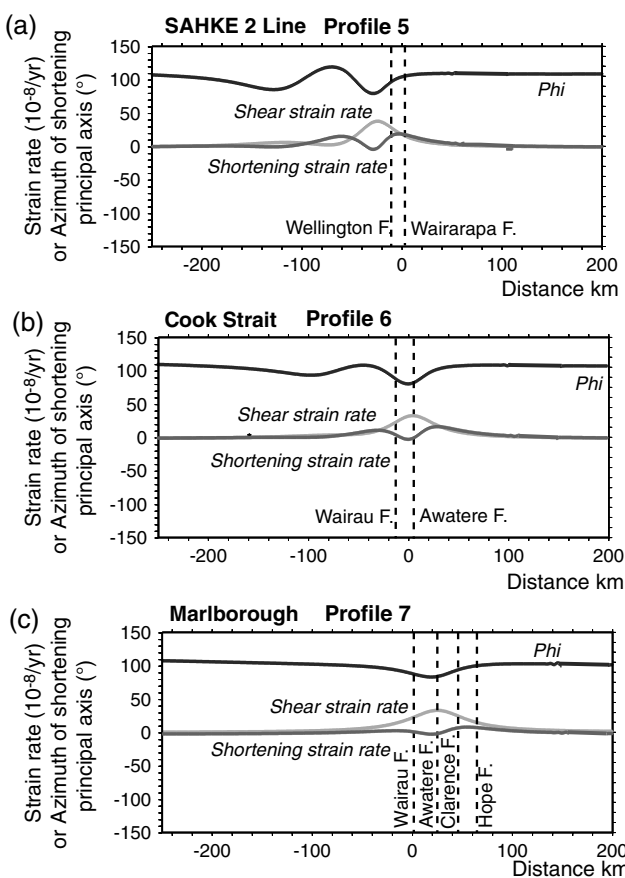


Figure 21. Plots for the southern Hikurangi margin showing shortening and shear strain rates (i.e., spatial gradients of shortening and shear velocities along the profiles), together with the azimuth of the horizontal shortening principal axis of strain rate (Φ), for dislocation models analyzed in this study. Because the dislocation models fit all components of the cGPS velocities well, they provide a good physical basis to smooth the velocity profiles in order to calculate velocity gradients. Note that peaks of horizontal shear and shortening strain rates do not coincide, implying some partitioning of the deformation. This is also reflected in the swings in the azimuth (Φ) of the principal shortening direction of horizontal strain rate along the profile. Also shown is the location of the surface trace of major faults, where they cross the line of the profile. See Figure 6 for profile locations. (a) SAHKE 2 line (Profile 5), using model with SSE in Figure 9; (b) Cook Strait (Profile 6) using model with SSE in Figure 11a; and (c) Marlborough in Figure 11b (Profile 7).

central Southern Alps, but erosion here absorbs most of the potential crustal thickening [Walcott, 1998].

[83] The present surface expression of the Alpine Fault, combined with microfabric studies, indicates that at shallow levels it dips at 45° – 60° [Norris and Cooper, 2001]. Thermobarometry studies on rocks in the immediate hanging wall show that they have been exhumed from depths of 20–30 km, with evidence for ductile deformation at temperatures $>300^\circ\text{C}$ and depths >7 km [Toy et al., 2010]. This is consistent with microseismicity studies [Boese et al., 2012] which show a marked cutoff in microseismicity near the Alpine

Fault at \sim 12 km depth. These studies suggest that we should anticipate freely slipping behavior of the fault at greater depths.

[84] Continuous GPS data for the central Southern Alps are confined to a transect in the Mt Cook region which has been operating for nearly 10 years (Figure 6, Profile 8). A feature of both the continuous GPS site velocities, and also campaign GPS data since the early 1990s [Beavan et al., 1999; Wallace et al., 2007], is that the shear component occurs over a relatively wide zone, extending up to \sim 80 km SE of the Alpine Fault.

7.2. Classical Back Slip Models

[85] A number of authors have used the “classical” back slip approach to model campaign GPS velocities across the central Southern Alps [Beavan et al., 1999, 2004, 2007; Wallace et al., 2007]. These require knowledge of the surface dips and slip vectors on the major faults in the region, but paradoxically, as discussed in section 3.2, the geometry of the

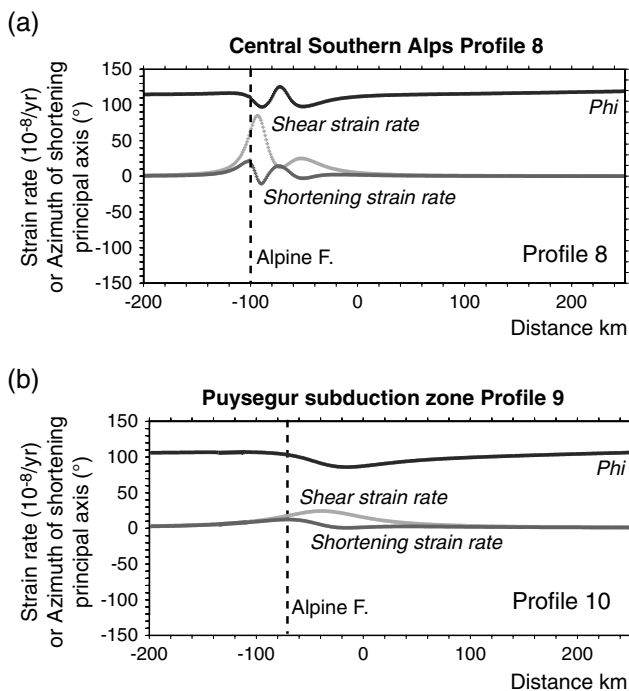


Figure 22. Plots for the central southern South Island showing shortening and shear strain rates (i.e., spatial gradients of shortening and shear velocities along the profiles), together with the azimuth of the horizontal shortening principal axis of strain rate (Φ), for the best fit dislocation models analyzed in this study. Because the dislocation models fit all components of the cGPS velocities well, they provide a good physical basis to smooth the velocity profiles in order to calculate velocity gradients. Note that peaks of horizontal shear and shortening strain rates do not coincide, implying some partitioning of the deformation. This is also reflected in the swings in the azimuth (Φ) of the principal shortening direction of horizontal strain rate along the profile. Also shown is the location of the surface trace of major faults, where they cross the line of the profile. See Figure 6 for profile locations. (a) Central southern Alps (Profile 8), using model in Figures 16c and 18; (b) Puysegur subduction zone (Profile 10) using model in Figure 20b.

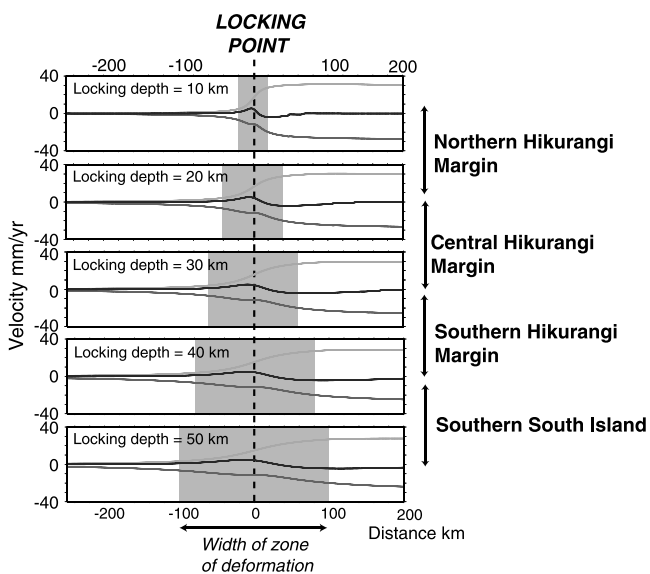


Figure 23. Plots showing theoretical profiles of shortening and shear velocities, using a typical dislocation model for the southern Hikurangi margin (Figures 2 and 6, Profile 5), but varying the locking depth between 10 and 50 km. They show that the width of the deforming zone, where gradients of interseismic velocity are significant, scales with approximately four times the locking depth. If the locking depth is determined by the onset of a marked velocity weakening mechanism during failure, then this suggests that the physical conditions that promote this mode of failure may play a fundamental role in determining the width of deformation in plate-boundary zones.

slipping parts is left unconstrained. The Alpine Fault dips $>45^\circ$, and this steep dip has a large effect on the modeling of both the component of shortening and vertical velocities. In order to fit the wide distribution of shear velocities, the models either invoke a deeply buried locking point for the Alpine Fault itself at >20 km depth [Beavan *et al.*, 1999; Wallace *et al.*, 2007] or a shallow locking point ~ 7 km depth together with slip on an antithetic fault with a much deeper locking point in the range 20–30 km [Beavan *et al.*, 2004]. Some of these models do not account for all of the relative plate convergence, as well as not satisfying the vertical motion boundary condition, but instead have the Pacific plate subsiding at ~ 2.5 mm/yr relative to the Australian plate [e.g., Beavan *et al.*, 2004].

[86] The model of Wallace *et al.* [2007] requires both a variable coupling factor beneath the locked part, decreasing to ~ 0.7 , and also additional specified internal deformation, and buried slip on an antithetic reverse fault that projects to the surface along the southeastern edge of the Southern Alps, with a dip-slip rate of nearly ~ 7 mm/yr. Given that in their model, this fault is explicitly assumed to have a surface expression, it is somewhat problematical, because there is no geological or topographic evidence for the required slip rates on any fault in the region. Beavan *et al.* [2010a] adjusted the dip of this putative back thrust to fit the vertical cGPS velocities.

[87] Moore *et al.* [2002] showed that the GPS velocity field in the central Southern Alps can also be modeled in terms of elastic straining above a distributed ductile shear zone. However, if the elastic lid is thin, then this requires nonuniform ductile shear, with shear strain rates increasing exponentially toward the fault. In section 3.5, we argue that nonuniform ductile shear requires a progressive decoupling between ductile and elastic deformation through the seismic

cycle [see also Savage, 2000], so it remains unclear whether these models are good descriptions of what is actually happening at depth.

7.3. Elastic Modeling in This Study

[88] Here we model the cGPS velocities in the central Southern Alps profile, using a similar approach to that used for the Hikurangi subduction zone, with a fault at depth, slipping at the relative plate motion. We emphasize that we make no assumptions or predictions about the long-term slip rates on any surface fault (especially the Alpine Fault) or rotation of the intervening fault blocks. Thus, the steady slip on a deeply buried fault may result in long-term faulting on many different surface faults, together with block rotation, and we cannot predict those faults, or any block rotation, from the interseismic velocity field alone. This is similar to the situation along the Hikurangi margin, where buried slip on deeper parts of the megathrust, over many seismic cycles, results in widespread long-term deformation in overlying plate, the details of which cannot be determined directly from the interseismic velocity field.

[89] In the context of the previous discussion, we now consider the possible range of models and their applicability to the deformation in central Southern Alps (Figures 15–18). Figure 18 shows our two alternative preferred best fit models in this study for the central Southern Alps.

7.3.1. A “Deep” Locking Point

[90] Slip at the relative plate motion on a single buried fault, with a locking depth of ~ 25 km, fits all components of the cGPS velocity field moderately well (average fits 1–1.7 mm/yr), involving either a “twist-down” tangential to a buried fault dipping at 20°SE , or a “twist-up” from a horizontal décollement at ~ 35 km depth. However, it is clear that these models do not fit the spatial gradients of any of the

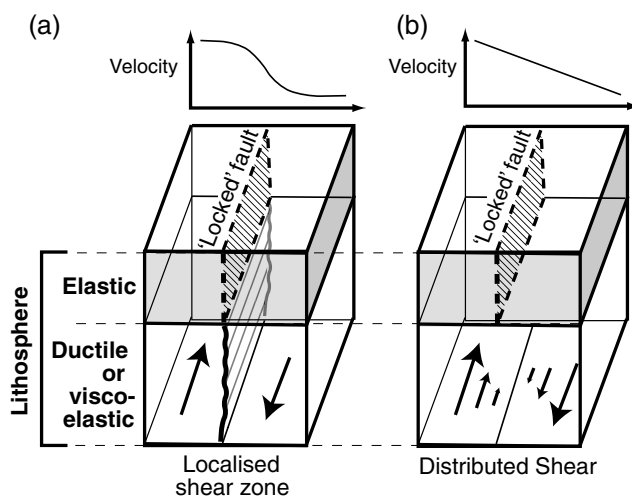


Figure 24. Cartoons showing two end member models for the interseismic behavior of the lithosphere at depth, beneath a major strike-slip fault. Here the fault ruptures during earthquakes, but is locked in the surface elastic layer during the interseismic period. (a) At depth in the lithosphere, beneath the “locked” zone, the fault may be undergoing creep on a narrow shear zone. In this case, elastic distortion in the elastic layer will show a clear interseismic geodetic signal of this deeper creep, defined by marked gradients in velocities close to the fault over a width which is roughly four times the locking depth (see Figure 23), or ~50 km for typical locking depths in the range 10–15 km. Note that this length scale is smaller than the width of the whole plate-boundary zone, such as that in New Zealand, and so that individual surface faults undergoing buried creep will result in local perturbations of the longer wavelength velocity field. (b) Alternatively, the deeper parts of the lithosphere may behave as a continuous viscoelastic material, so that during the interseismic period, there is elastic straining in a wide zone beneath the “locked” fault, which relaxes as permanent creep. In this case, there will be no interseismic geodetic signal associated with the surface fault, and the fault during this period does not “exist,” and the long wavelength velocity field across the plate-boundary will only be controlled by the location of the locking point on the plate interface.

components of velocities close to the Alpine Fault (Figure 15). The models also remain unsatisfactory because the locking point is significantly deeper than that suggested by both microseismicity and the pressure-temperature conditions of rocks exhumed on the Alpine Fault (see section 7.1).

7.3.2. A “Shallow” Locking Point

[91] A shallow locking point (7–12 km), with either a “twist-up” or “twist-down,” clearly has a poor fit with the component of horizontal motion perpendicular to the profile (shear component), with too high shear velocities at distances >15 km SE of the Alpine Fault (Figure 16a). However, for a locking depth of 12 km, it matches the gradients of velocity close to the fault well. This strongly suggests that the locking point is shallow, but something other than just steady slip must happen at depth. It is worth noting that there is no evidence of SSEs in any of the cGPS sites along Profile 8. Thus, a solution which matches the cGPS data involves a second locked patch (multilocking point model), defining an additional locked patch at depths of ~25 km, and between 25 and 40 km SE of the outcrop of the Alpine Fault (Figures 16b and 18a). In this case, the “twist-up” model matches all the velocity components and their gradients well, with an average misfit ~1 mm/yr. This model requires the slipping fault to merge with a subhorizontal ductile décollement at Moho depth (35 km), about 100 km SE of the Alpine Fault, indicating significant underthrusting of the Australian plate beneath the Pacific plate. We note that the location of a deeper locked patch shows a correlation with a high resistivity gap between two patches of low resistivity (Figure 19), documented by Wannamaker *et al.* [2009]

[92] As a further test of our “twist-up model,” we use a conventional back slip approach with the same geometry as our shallow locking point model (Figure 17a). It is clear that this fails to match the vertical velocities or satisfy the plate-boundary conditions. In order to test whether having more than one buried slipping fault is a better model, we consider a modification of our multilocking point model. Here instead of a “twist-up,” there is a buried planar antithetic fault (Figure 17b). This results in a significantly worse fit to both the shortening and vertical components of velocity. We therefore reject this type of model.

7.3.3. Shallow Locking Point and Deeper Distributed Shear

[93] We also consider the possibility of elastic deformation being driven by underlying and distributed ductile shear, as suggested by Moore *et al.* [2002]. We model this by varying the apparent coupling factor along the free slipping zone, where the elastic effect of the zone of distributed shear is described by a linearly decreasing coupling factor, reaching zero at the edge of the shear zone. Figures 17c and 18b show a twist-up model, but with ~9 mm/yr of distributed dextral ductile shear at depths >25 km (coupling factor increasing from 0 to 0.25). This passes upward and toward the NW into a free slipping fault, moving at ~0.75 times the plate convergence rate (~29 mm/yr of dextral shear).

[94] Note that this is an “ad hoc” model, and not necessarily physically realistic, because it involves imposing both a reduced slip rate on the freely slipping part of the fault and a specified amount of elastic deformation that is driven by deeper ductile flow. This model does not require a locked

patch at depth. The fit is essentially the same as the best fit twist-up shallow locking with a deep “locked patch” model (Figure 18a and section 7.3.2) and is therefore a potential alternative model of deformation beneath the southern Alps that also requires significant underthrusting of the Australian plate SE of the Alpine Fault (Figure 18b).

8. Puysegur Subduction Zone

[95] Farther south, in Fiordland, displacement on the Alpine Fault is transferred offshore to the west, in the Puysegur subduction zone (Figure 6). Here subduction has the opposite polarity to the Hikurangi margin, so that Australian oceanic lithosphere and thinned continental lithosphere are being subducted toward the east beneath southern South Island [Walcott, 1998]. The overlying Pacific plate in Central Otago, up to 300 km east of the trench, is cut by a series of Late Miocene to recent active reverse block faults, spaced 15–20 km, trending subparallel to trench. These have accommodated <10 km of shortening [Norris, 2004].

[96] The seismic Benioff Zone is well defined where the Puysegur subduction zone underlies southwestern South Island. This shows that at depths of ~50 km, the subducted plate dips at ~50° within 50 km of the trench, and below 100 km is subvertical to overturned (Figure 20). The subduction megathrust here has experienced two earthquakes $>M7$ since 2003, with $M7.2$ in 2003 and $M7.8$ in 2009 (Figure 6). These were the result of rupture of the megathrust down to a depth of ~50 km beneath southern Fiordland [Beavan *et al.*, 2010b]. The 2009 earthquake had an oblique slip vector, subparallel to the Pacific/Australian plate motion, whereas the 2003 earthquake had a slightly greater thrust component [Beavan *et al.*, 2010b].

8.1. Elastic Modeling of the Puysegur Subduction Zone

[97] Continuous GPS sites in the southern part of South Island are very sparse with ~100 km spacing, and sites within 300 km of the Puysegur trench only started recording after the 2003 $M7.2$ Fiordland earthquake. The cGPS sites around Dunedin have been recording for much longer, but are sufficiently far from the Fiordland region that their long-term velocities are within 2 mm/yr of the Pacific plate. In this study, we only consider GPS time series prior to the 2009 $M7.8$ earthquake. In this earthquake, there was up to 1 m of elastic rebound over most of southern South Island, significantly perturbing the long-term regional GPS velocities.

[98] We use published campaign GPS transect [Wallace *et al.*, 2007] for Profile 9 (Figures 1a and 6), and cGPS data for Profile 10 (Figure 6). There may be a problem with the reference frame for the campaign data, because it suggests ~2.5 mm/yr margin parallel shear with respect to the Pacific plate east of Dunedin (Figure 20a) [Beavan *et al.*, 2002; Wallace *et al.*, 2007], which is not apparent in over 10 years of cGPS data (Figure 20b). In any case, it is clear with the available data that the entire cGPS velocity field across southern South Island can be modeled by a single locking point on the Puysegur megathrust at a depth of 45–50 km (Figure 20), consistent with the maximum depth of rupture of the 2009 $M7.8$ Dusky Sound earthquake (Figure 6). Unfortunately, the dearth of cGPS sites in the critical region close to the locking point, where velocity gradients are maximum, means that this model is not well constrained.

However, given the wide region of elastic rebound in the 2009 earthquake, up to several hundred kilometers from the epicenter, it is consistent with the known seismic cycle in this part of the subduction zone.

9. Discussion

[99] The success of the simple twist model used in this study to fit the short-term velocity field in the New Zealand plate-boundary zone is remarkable, given the width of the deforming plate-boundary zone, up to 250 km wide, and the complexity of active surface faulting. In our view, this is strong evidence that the short-term interseismic deformation reflects the fundamental driving force of deformation at depth. Here the boundary between the plates is a single interface with movement at the relative plate convergence.

9.1. Relation Between Short-Term Velocity Field and Long-Term Deformation

[100] We would anticipate, as Walcott [1984] was the first to show, that the pattern of geodetic strain rate—in other words, the spatial gradient in velocity—will mirror to some extent the long-term style of faulting. Indeed, the ability of the multiblock models of Wallace *et al.* [2004, 2007, 2012a] to reproduce this is a further demonstration of this.

9.1.1. Components of Strain Rate

[101] Figures 21 and 22 show the shear and shortening components of strain rate along the various profiles analyzed in this study (located in Figure 6), as well as the azimuth (phi) of the principal shortening axis of strain rate. One might anticipate the regions of highest shear strain to be associated strike-slip faulting. Here there is an obvious broad scale link, with the major strike-slip faults occurring in regions of increased shear strain.

[102] However, in detail, Figures 21 and 22 show that the locus of maximum shear strain rate need not coincide with the surface trace of the strike-slip faults with most rapid long-term slip rates. For example, in southern and central South Island (Profiles 8 and 10), the Alpine Fault lies 7–30 km NW of the region of peak shear strain rate (Figure 22b). For the profile across the northeastern part of South Island (Figure 21c, Profile 7), straddling the Marlborough Fault Zone (Figures 2 and 6), the peak shear strain rate coincides with the surface trace of the Awatere Fault, which has a long-term Holocene dextral slip rate of ~6 mm/yr [Little *et al.*, 1998]. However, the most rapidly slipping fault here is the Hope Fault (>20 mm/yr dextral), which is located ~35 km farther SE (Figure 21c). The same feature can be observed farther north with the Wairarapa Fault (Figure 21a, Profile 5), which is the most rapidly slipping fault in southern North Island, with a Holocene dextral rate of ~10 mm/yr [Little *et al.*, 2009], but lies ~30 km SE of the zone of peak shear strain rate. In fact, the Wellington and Wairarapa Faults together account for ~75% of the long-term relative motion parallel to this part of the plate-boundary zone.

[103] The location of the peak shear strain rate in most profiles is determined by the horizontal position of the locking point on the slipping part of the plate interface in that profile (partial slip as a consequence of SSEs or multiple locking points will slightly modify this). With dipping faults,

even if they intersect the locking point at a depth, the peak shear strain rate will be offset relative to their surface trace. In the case of the Wairarapa Fault in southern North Island, or the Hope and central Alpine Fault in South Island (Figure 2), it is plausible that the downdip projections of these fault do indeed intersect the locking point (requiring dips in the range 45° – 60° and/or listric geometries), and this may explain why these are such rapidly slipping faults, because in many respects, they may be direct extensions of the deeper and freely slipping plate interface. However, this does not seem to be the case for the southern part of the Alpine Fault (Profile 10), which is subvertical in surface trace, indicating that the position and slip rate of major faults is also controlled by the local strength of the crust and/or mantle, presumably related to their geological history.

9.1.2. Partitioning of Deformation

[104] Partitioning of the long-term deformation in the southern and central part of the Hikurangi margin is evident, with mainly margin parallel dextral shear along the North Island Shear Belt, and mainly thrusting farther east (Figures 2 and 6) [Lamb and Vella, 1987]. To some extent, this partitioning can also be seen in the short-term geodetic velocity field [Walcott, 1984; Lamb and Vella, 1987; Darby and Beavan, 2001], although it is less marked. This is illustrated in Figure 21a for the SAHKE 2 line (Figures 2 and 6, Profile 5), where the locations of maximum shortening and shear strain rates (i.e., maximum positive gradients of shortening and shear velocities) along the profile do not coincide. Thus, the peak shear strain rate occurs west of the Wellington Fault (at a distance along the profile of -30 km), whereas the peak (most positive) shortening strain rate occurs at distances of -5 and -50 km. This is also reflected in the swings in the azimuth (ϕ) of the principal direction of horizontal strain along the profile. However, the governing equations of isotropic elasticity require some partitioning of the shear and shortening components in the interseismic velocity field, even if all motion is accommodated by uniform slip on the megathrust [Bevis and Martel, 2001]. Thus, one should be wary of comparing the local orientation of the GPS-derived strain rate tensor with the style of finite deformation and there could be considerable differences between the two.

[105] Big earthquakes, involving large ruptures on deep faults, will release elastic stresses over a wide region, extending for hundreds of kilometers. For example, some of the strong shortening strain accumulating in southern North Island (Figures 21a and 21b) must ultimately be released offshore, to the east, because the long-term rate of onshore thrusting is too low to accommodate it all [Lamb and Vella, 1987]. In southern South Island, the regional pattern of elastic strain accumulation can be related to locking on the Puysegur subduction zone (Figures 6 and 20), and presumably most of this will end up as slip on the subduction megathrust, with only a small residual left behind to drive more local faulting. In this case, GPS velocities here cannot be used to constrain local long-term strain rates, such as across Central Otago where Plio-Pleistocene and active reverse block faulting is occurring—in other words, these faults are effectively “invisible” in the cGPS velocity field.

9.2. Width of Interseismic Plate-Boundary Zone

[106] The simple locking point model in this study has proved successful at capturing the cGPS velocity field. It is

easy to show that the depth of the locking point is directly related to the characteristic width of the zone accumulating elastic strain. As a rule of thumb, the width of the zone of significant strain rate is ~ 4 times the locking point depth, illustrated in Figure 23 for a typical central Hikurangi margin geometry. Thus, the progressive southward deepening of the locking point along the megathrust in the Hikurangi subduction zone, from <10 km in offshore the northeastern North Island, to ~ 35 km beneath northeastern South Island, implies a widening of the zone of significant strain rate associated with plate convergence from <50 to ~ 150 km. Back-arc extension in North Island complicates the picture, but the region of strain accumulation associated with this extension lies ~ 200 km west of the region accumulating compressional strain, which is why the intervening region can be described on the GPS time scale as a coherent quasi-rigid domain.

[107] The fact that the width of the zone of elastic strain is comparable to the width of the zone of finite strain over millions of years suggests that the link with locking point depth has profound consequences for the evolution of the plate-boundary zone. From a dynamical point of view, the really important controlling factor for the locking point location is stick-slip behavior on faults. Specifically, the important question is what determines the change in mode of brittle failure from a plastic type failure to velocity weakening. At depth, where the fault is undergoing steady slip as a consequence of plastic-type failure, fault stresses must be relieved at essentially the rate that they are accumulating. However, above the locking point, stresses on the fault will be constantly increasing, driven by the deeper steady state slip. Eventually, this part of the fault will reach failure and rupture during an earthquake. However, velocity weakening during the rupture will allow stresses on the fault to drop well below the initial failure stress. This way, there is a requirement for an interseismic period with enough time during the locked phase to allow stresses to build up again to failure.

[108] The transition from plastic-type to velocity weakening failure is likely to be related to changes in any or all of the following: lithology, temperature, pressure, fluid pressure, and stress/strain accumulation rate. However, the relationships remain unclear. Lamb [2006] showed from a simultaneous inversion for temperature and shear stress along 11 different subduction megathrusts (including the central part of the Hikurangi margin), constrained by the force balance across the subduction zone, that this transition often occurs at temperatures $<200^{\circ}\text{C}$, and well below that expected for a true brittle/ductile transition. Heat flow data in the Hikurangi margin suggest similar low temperatures [McCaffrey *et al.*, 2008].

9.3. SSEs and Locking Points

[109] We have shown that the model fit to the observed cGPS velocities along the Hikurangi margin, particularly the vertical motions, is improved by taking account of slow slip events. Here we have incorporated the effect of SSEs by an apparent partial coupling factor, which describes incomplete averaging of the full seismic cycle, as discussed in section 5.2. Our analysis resolves a patch of the subduction megathrust, downdip of the locking point, where SSEs are occurring, with an intervening region that appears geodetically to be essentially freely slipping (Figures 6 and 14). As discussed in section 9.2, the locking point must represent a change from plastic-type failure to failure with strong

velocity weakening, and this occurs at relatively low temperatures ($<200^{\circ}\text{C}$), well below the true brittle/ductile transition. The presence of SSEs suggests that velocity weakening again becomes a mechanism of failure farther downdip, although the nonseismic nature of the failure requires less effective velocity weakening, on a longer time scale, promoting slip over an extended period of days to months. The downdip termination of SSEs may be sufficiently hot that it is the true brittle/ductile transition.

[110] There is a suggestion in the profile along the SAHKE 2 line (Figures 2 and 6, Profile 5), where the lithospheric structure is well imaged, that the updip limit of SSEs coincides with the crust-mantle boundary (Figure 9). This provides a natural explanation for the reemergence of velocity weakening at greater depth, determined by lithology. Interestingly, updip of this, the main locking point occurs at the western edge of a body of crust with anomalously low P wave velocities (Tozer, unpublished thesis, 2012), which might be underplated sediment. In the northern part of the Hikurangi margin, the main locking point is at much shallow depths (7–15 km) (Figure 6, Profiles 1–3), and SSEs occur in the crustal part of the megathrust. The reasons for this are unclear, but must be important for our understanding of the earthquake process.

[111] Our shallow locking point dislocation modeling in the central Southern Alps (section 7.3.2 and Figure 18a) also requires a deep patch of locked plate interface downdip of the main shallow locking point. This could be no more than a region prone to SSEs, but the time span of geodetic studies suggests a repeat time >20 years. However, the high thermal gradient [Toy *et al.*, 2010] suggests that the main shallow locking point is the brittle-ductile transition. A plausible explanation for the deeper locking point is that it occurs in a region of embrittlement at high pore fluid pressure, which results in a return to brittle behavior at higher temperatures and pressures. In this case, the failure stress here will be lower than that on the shallower brittle fault, and so even if it ruptures seismically, it is likely to have an earthquake repeat time less than the surface faults. However, during major earthquakes, both shallow and deeper parts may rupture together, and so the total moment release may be greater than would be predicted if brittle faulting is restricted to the top 12 km or so.

9.4. The Role of Faults

[112] The general lack of evidence for creep at depth beneath individual locked surface strike-slip or thrust faults in the New Zealand plate-boundary zone, other than the plate interface itself, is perhaps surprising given their large strike-slip displacements, between tens and hundreds of kilometers. Even where there is oblique continental collision, in the Southern Alps, the deeper slipping part of the plate-boundary cannot be uniquely associated with the Alpine Fault, but rather underlies a wider region of faulting and possibly block rotation. This is different to elsewhere in the world, where localized marked gradients of velocity in the interseismic deformation across major continental strike-slip faults indicate active localized and buried creep at depths of 10–20 km—for example, the North Anatolian Fault [Wright *et al.*, 2001], Denali Fault [Freymueller *et al.*, 2008], Altyn Tagh Fault [Wright *et al.*, 2004], or San Andreas Fault System [Smith-Konter *et al.*, 2011].

[113] Thus, the question remains: what happens at depth beneath major surface faults, such as those in New Zealand, that do not show geodetic evidence for buried creep (Figure 24). One possibility is that here the whole lithosphere behaves as a viscoelastic material. Thus, between earthquakes, and away from the slipping parts of the plate interface, there is no focused shear at depth, but rather some sort of lithospheric flow which follows the overlying elastic distortion, but eventually becomes permanent. During an earthquake, the brittle portions must effectively decouple themselves from this underlying flow, resulting in discrete offsets on surface faults. The pattern of mantle deformation from shear wave splitting beneath South Island is consistent with this, suggesting a more distributed pattern of mantle deformation, rather than only slip on discrete shear zones [Molnar *et al.*, 1999; Moore *et al.*, 2002].

10. Conclusions

[114] In this study we analyze the short-term interseismic velocity field in the New Zealand plate-boundary zone, revealed by cGPS measurements over the last decade. We use a new method of back slip analysis [Savage, 1983], involving twist-up or twist-down on cylindrical virtual faults, to show the following:

[115] 1. Despite a complex pattern of rapid active surface faulting and block rotation, over periods of thousands of years, and involving geological displacements up to hundreds of kilometers on individual faults, almost the entire plate-boundary continuous GPS velocity field, both *horizontal* and *vertical* components, over the past \sim 10 years, can be predicted within measurement error by a simple model of elastic distortion due to deep slip at the *relative plate motion rates*, on a *single* plate interface, which is the subduction megathrust in the Hikurangi and Puysegur margins.

[116] 2. Along the Hikurangi Margin, deformation involves a twist-down of the Pacific plate. The depth of the locking point on the subduction megathrust becomes progressively deeper toward the south, from 5 to 15 km in the northern part of the margin, to \sim 35 km in the southernmost part.

[117] 3. A locking point depth in the range 45–50 km is required in the Puysegur subduction megathrust.

[118] 4. Vertical-axis rotation in the northern plate-boundary is also required to fit the velocities. Here an \sim 150 km long segment of the fore arc, referred to as the Wairoa domain, rotates clockwise at $4.5^{\circ} \pm 1$ Ma, relative to the Australian plate, about a pole in western North Island.

[119] 5. The remnant parts of the velocity field along the Hikurangi Margin are mainly a result of incomplete averaging of the cycle of slow slip events (SSEs) on the plate interface, downdip of the locking point, and can be modeled by an “apparent coupling factor” of 1 or <0.5 .

[120] 6. The best fit model for interseismic velocities along the Southern Alps involves a twist-up of the Pacific plate, with free slip on the plate interface at \sim 12 km depth to the SE of the surface trace of the Alpine Fault. Deeper on the plate interface, surface velocities are well matched by either a “locked patch” at \sim 25 km depth and 25–45 km SE of the Alpine Fault, or a zone of distributed shear at depths $>$ 25 km and 50–100 km SE of the Alpine Fault.

[121] 7. There is no resolvable evidence in the interseismic deformation, given the uncertainties, for buried creep in shear

zones at depth beneath individual locked surface faults, other than on the plate interface itself. Therefore, knowledge of surface fault slip rates/geometry is not required to model GPS velocity field. In the interseismic period, the main driving force of plate-boundary deformation is deep slip on the deeper moving part of the plate interface. This causes a steady build up in tectonic stress in the elastic layer, which will ultimately be relieved during earthquakes by slip on a complex array of crustal faults.

[122] **Acknowledgments.** This paper would not have been possible without the pioneering work of John Beavan, who laid the foundations of GPS observation and interpretation in the New Zealand plate-boundary for tectonic analysis. John Beavan sadly passed away in November 2012, but his work will live on.

References

- Ader, T., et al. (2012), Convergence rate across the Nepal Himalaya and interseismic coupling on the Main Himalayan Thrust: Implications for seismic hazard, *J. Geophys. Res.*, **117**, B04403, doi:10.1029/2011JB009071.
- Beavan, J., et al. (1999), Crustal deformation during 1994–1998 due to oblique continental collision in the central Southern Alps, New Zealand, and implications for seismic potential of the Alpine Fault, *J. Geophys. Res.*, **104**, 25233–25255.
- Beavan, J., P. Tregoning, M. Bevis, T. Kato, and C. Meertens (2002), Motion and rigidity of the Pacific plate and implications for plate boundary deformation, *J. Geophys. Res.*, **107**(B10), 2261, doi:10.1029/2001JB000282.
- Beavan, J., D. Matheson, P. Denys, M. Denham, T. Herring, B. Hager, and P. Molnar (2004), A vertical deformation profile across the Southern Alps, New Zealand, from 3.5 years of continuous GPS data, in Proceeding of the Workshop, *The State of GPS Vertical Positioning Precision: Separation of Earth Processes by Geodesy*, Cahiers du Centre Européen de Géodynamique et de Séismologie, 23, edited by T. van Dam and O. Francis, pp. 111–123, Centre Européen de Géodynamique et de Séismologie, Luxembourg.
- Beavan, J., S. Ellis, L. Wallace, and P. Denys (2007), Kinematic constraints from GPS on oblique convergence of the Pacific and Australian plates, central South Island, New Zealand, in *A Continental Plate Boundary: Tectonics at South Island, New Zealand*, Geophys. Monogr. Ser., vol. 175, edited by D. Okaya, T. Stern, and F. Davey, pp. 75–94, AGU, Washington, D. C., doi:10.1029/175GM05.
- Beavan, J., P. Denys, M. Denham, B. Hager, T. Herring, and P. Molnar (2010a), Distribution of present-day vertical deformation across the Southern Alps, New Zealand, from 10 years of GPS data, *Geophys. Res. Lett.*, **37**, L16305, doi:10.1029/2010GL044165.
- Beavan, J., S. Samsonov, P. Denys, R. Sutherland, N. Palmer, and M. Denham (2010b), Oblique slip on the Puysegur subduction interface in the 2009 July M_w 7.8 Dusky Sound earthquake from GPS and InSAR observations: Implications for the tectonics of southwestern New Zealand, *Geophys. J. Int.*, **183**, 1265–1286, doi:10.1111/j.1365-246X.2010.04798.x.
- Berryman, K. R., S. Beanland, A. F. Cooper, H. N. Cutten, R. J. Norris, and P. R. Wood (1992), The Alpine Fault, New Zealand, variation in Quaternary structural style and geomorphic express, *Ann. Tecton.*, **6**, 126–163.
- Berryman, K., Y. Ota, T. Miyachi, A. Hull, K. Clark, K. Ishibashi, N. Iso, and N. Litchfield (2011), Holocene paleoseismic history of upper plate faults in the southern Hikurangi subduction margin, New Zealand, deduced from marine terrace records, *Bull. Seismol. Soc. Am.*, **101**, 2064–2087, doi:10.1785/0120100282.
- Bevis, M. (1986), The curvature of Wadati-Benioff zones and the torsional rigidity of subducting plates, *Nature*, **323**, 52–53, doi:10.1038/323052.
- Bevis, M., and S. Martel (2001), Oblique plate convergence and interseismic strain accumulation, *Geochem. Geophys. Geosyst.*, **2**, 1033, doi:2000GC000125, (Available at <http://g-cubed.org>)
- Boese, C. M., J. Townsend, E. Smith, and T. Stern (2012), Microseismicity and stress in the vicinity of the Alpine Fault, central Southern Alps, New Zealand, *J. Geophys. Res.*, **117**, B02302, doi:10.1029/2011JB008460.
- Cowan, H. A. (1990), Late Quaternary displacements on the Hope Fault at Glynn Wye, North Canterbury, *N. Z. J. Geol. Geophys.*, **33**, 285–293.
- Darby, D. J., and J. Beavan (2001), Evidence from GPS measurements for contemporary plate coupling on the southern Hikurangi subduction thrust and partitioning of strain in the upper plate, *J. Geophys. Res.*, **106**, 30,881–30,891, doi:10.1029/2000JB000023.
- Eberhart-Phillips, D., M. Chadwick, and S. Bannister (2008), Three-dimensional attenuation structure of central and southern South Island, New Zealand, from local earthquakes, *J. Geophys. Res.*, **113**, B05308, doi:10.1029/2007JB005359.
- England, P. C., and G. A. Houseman (1989), Extension during continental convergence, with application to the Tibetan Plateau, *J. Geophys. Res.*, **94**, 17561–17579.
- England, P. C., and D. P. McKenzie (1982), A thin viscous sheet model for continental deformation, *Geophys. J. R. Astron. Soc.*, **70**, 295–321. (Correction to A thin viscous sheet model for continental deformation, *Geophys. J. R. Astron. Soc.*, **73**, 523–532, 1983.)
- Freymueller, J. T., H. Woodard, S. Cohen, R. Cross, J. Elliott, C. Larsen, S. Hreinsdóttir, and C. Zweck (2008), Active deformation processes in Alaska, based on 15 years of GPS measurements, in *Active Tectonics and Seismic Potential of Alaska*, AGU Geophysical Monograph, 179, edited by J. T. Freymueller, P. J. Haessler, R. Wesson, and G. Ekstrom, pp. 1–42, AGU, Washington, D. C.
- Jackson, J. (2002), Strength of the continental lithosphere: Time to abandon the jelly sandwich?, *GSA Today*, **12**(9), 4–10, doi:10.1130/1052-5173.
- Kanda, R. V. S., and M. Simons (2010), An elastic plate model for interseismic deformation in subduction zones, *J. Geophys. Res.*, **115**, B03405, doi:10.1029/2009JB006611.
- Kanda, R. V. S., and M. Simons (2012), Practical implications of the geometrical sensitivity of elastic dislocation models for field geologic surveys, *Tectonophysics*, **560–561**, 94–104.
- Lamb, S. H. (1994), Behavior of the brittle crust in wide zones of deformation, *J. Geophys. Res.*, **99**, 4457–4483.
- Lamb, S. H. (2002), Is it all in the crust?, *Nature*, **420**, 130–131.
- Lamb, S. (2006), Shear stresses on megathrusts: Implications for mountain building behind subduction zones, *J. Geophys. Res.*, **111**, B07401, doi:10.1029/2005JB003916.
- Lamb, S. (2011), Cenozoic tectonic evolution of the New Zealand plate-boundary zone: A paleomagnetic perspective, *Tectonophysics*, **30**, doi:10.1016/j.tecto.2011.06.005.
- Lamb, S., and P. Vella (1987), The last million years of deformation in part of the New Zealand plate-boundary zone, *J. Struct. Geol.*, **9**, 877–891.
- Little, T. A., R. Grapes, and G. W. Berger (1998), Late Quaternary strike-slip on the eastern part of the Awatere fault, South Island, New Zealand, *Geol. Soc. Am. Bull.*, **110**(2), 127–148, doi:10.1130/0016-7606(1998).
- Little, T. A., R. Van Dissen, E. Schermer, and R. Carne (2009), Late Holocene surface ruptures on the southern Wairarapa fault, New Zealand: Link between earthquakes and the uplifting of beach ridges on a rocky coast, *Lithosphere*, **1**, 4–28, doi:10.1130/L7.1.
- McCaffrey, R. (2002), Crustal block rotations and plate coupling, in *Plate Boundary Zones*, AGU Geodyn. Ser., vol. 30, edited by S. Stein, and J. Freymueller, pp. 100–122, AGU, Washington, DC.
- McCaffrey, R. (2005), Block kinematics of the Pacific-North America plate boundary in the southwestern United States from inversion of GPS, seismological, and geologic data, *J. Geophys. Res.*, **110**, B07401, doi:10.1029/2004JB003307.
- McCaffrey, R., M. D. Long, C. Goldfinger, P. C. Zwick, J. L. Nabelek, C. K. Johnson, and C. Smith (2000), Rotation and plate locking at the southern Cascadia subduction zone, *Geophys. Res. Lett.*, **27**, 3117–3120.
- McCaffrey, R., A. I. Qamar, R. W. King, R. Wells, G. Khazaradze, C. A. Williams, C. W. Stevens, J. J. Vollink, and P. C. Zwick (2007), Fault locking, block rotation and crustal deformation in the Pacific Northwest, *Geophys. J. Int.*, **169**, 1315–1340, doi:10.1111/j.1365-246X.2007.03371.x.
- McCaffrey, R., L. M. Wallace, and J. Beavan (2008), Slow slip and frictional transition at low temperature at the Hikurangi subduction zone, *Nat. Geosci.*, **1**, 316–320.
- McKenzie, D. P., and J. A. Jackson (1983), The relationship between strain rates, crustal thickening, paleomagnetism, finite strain and fault movements within a deforming zone, *Earth Planet. Sci. Lett.*, **65**, 182–202.
- Molnar, P., et al. (1999), Continuous deformation versus faulting through the continental lithosphere of New Zealand, *Science*, **286**, 516–519.
- Moore, M., P. England, and B. Parsons (2002), Relation between surface velocity field and shear wave splitting in the South Island of New Zealand, *J. Geophys. Res.*, **107**(B9), 2198, doi:10.1029/2000JB000093.
- Norris, R. J. (2004), Strain localisation within ductile shear zones beneath active faults: The Alpine Fault contrasted with the adjacent Otago Fault System, New Zealand, *Earth Planets Space*, **56**, 1095–1101.
- Norris, R. J., and A. F. Cooper (2001), Late Quaternary slip rates and slip partitioning on the Alpine Fault, New Zealand, *J. Struct. Geol.*, **23**, 507–520, doi:10.1016/S0191-8141(00)00122-X.
- Okada, Y. (1985), Surface deformation due to shear and tensile faults in a half-space, *Bull. Seismol. Soc. Am.*, **75**, 1135–1154.
- Okada, Y. (1992), Internal deformation due to shear and tensile faults in a half-space, *Bull. Seismol. Soc. Am.*, **82**, 1018–1040.
- Prescott, W., and A. Nur (1981), The accommodation of relative motion at depth on the San Andreas Fault System in California, *J. Geophys. Res.*, **86**, 999–1004.
- Reyners, M., D. Eberhart-Phillips, and S. Bannister (2011), Tracking repeated subduction of the Hikurangi Plateau beneath New Zealand, *Earth and Planetary Science Letters*, **311**, 165–171.

LAMB AND SMITH: MODELING GPS VELOCITIES IN NEW ZEALAND

- Savage, J. C. (1983), A dislocation model of strain accumulation and release at a subduction zone, *J. Geophys. Res.*, *88*, 4984–4996.
- Savage, J. C. (2000), Viscoelastic coupling model for the earthquake cycle driven from below, *J. Geophys. Res.*, *105*, 25,525–25,532.
- Schwartz, S. Y., and J. M. Rokosky (2007), Slow slip events and seismic tremor at circum-Pacific subduction zones, *Rev. Geophys.*, *45*, RG3004, doi:10.1029/2006RG000208.
- Smith-Konter, B. R., D. T. Sandwell, and P. Shearer (2011), Locking depths estimated from geodesy and seismology along the San Andreas Fault System: Implications for seismic moment release, *J. Geophys. Res.*, *116*, B06401, doi:10.1029/2010JB008117.
- Toy, V. G., D. Craw, A. Cooper, and R. Norris (2010), Thermal regime in the central Alpine Fault zone, New Zealand: Constraints from microstructures, biotite chemistry and fluid inclusion data, *Tectonophysics*, *485*, 178–192.
- Vergne, J., R. Cattin, and J. P. Avouac (2001), On the use of dislocations to model interseismic strain and stress build-up at intracontinental thrust faults, *Geophys. J. Int.*, *147*, 155–162.
- Walcott, R. I. (1984), The kinematics of the plate boundary zone through New Zealand: A comparison of short- and long-term deformations, *Geophys. J. R. Astron. Soc.*, *79*, 613–633.
- Walcott, R. I. (1998), Modes of oblique compression: late Cenozoic tectonics of the South Island of New Zealand, *Rev. Geophys.*, *36*, 1–26.
- Wallace, L., and J. Beavan (2010), Diverse slow slip behavior at the Hikurangi subduction margin, New Zealand, *J. Geophys. Res.*, *115*, B12402, doi:10.1029/2010JB007717.
- Wallace, L., P. Barnes, J. Beavan, R. Van Dissen, N. Litchfield, J. Mountjoy, R. Langridge, G. Lamarche, and N. Pondard (2012a), The kinematics of a transition from subduction to strike-slip: An example from the central New Zealand plate boundary, *J. Geophys. Res.*, *117*, B02405, doi:10.1029/2011JB008640.
- Wallace, L., J. Beavan, S. Bannister, and C. Williams (2012b), Simultaneous long-term and short-term slow slip events at the Hikurangi subduction margin, New Zealand: Implications for processes that control slow slip event occurrence, duration, and migration, *J. Geophys. Res.*, *117*, B11402, doi:10.1029/2012JB009489.
- Wallace, L. M., J. Beavan, R. McCaffrey, and D. Darby (2004), Subduction zone coupling and tectonic block rotation in the North Island, New Zealand, *J. Geophys. Res.*, *109*, B12406, doi:10.1029/2004JB003241.
- Wallace, L. M., R. J. Beavan, R. McCaffrey, K. R. Berryman, and P. Denys (2007), Balancing the plate motion budget in the South Island, New Zealand using GPS, geological and seismological data, *Geophys. J. Int.*, *168*(1), 332–352, doi:10.1111/j.1365-246X.2006.03183.x.
- Wallace, L. M., et al. (2009), Characterizing the seismogenic zone of a major plate boundary subduction thrust: Hikurangi margin, New Zealand, *Geochem. Geophys. Geosyst.*, *10*, Q10006, doi:10.1029/2009GC002610.
- Wannamaker, P. E., T. Caldwell, G. Jiracek, V. Maris, G. Hill, Y. Ogawa, H. Bibby, S. Bennie, and H. Wiebke (2009), Fluid and deformation regime of an advancing subduction system at Marlborough, New Zealand, *Nature*, *460*, 733–736, doi:10.1038/nature08204.
- Wech, A., C. Boese, T. Sten, and J. Townend (2012), Tectonic tremor and deep slow slip on the Alpine Fault, *Geophys. Res. Lett.*, *39*, L10303, doi:10.1029/2012GL051751.
- Wright, T., B. Parsons, and E. Fielding (2001), Measurement of interseismic strain accumulation across the North Anatolian Fault by satellite radar interferometry, *Geophys. Res. Lett.*, *28*, 2117–2120.
- Wright, T. J., B. Parsons, P. C. England, and E. J. Fielding (2004), InSAR observations of low slip rates on the major faults of western Tibet, *Science*, *305*, 236–239.